1 Response to reviewer comments

In the following, we provide a point-by-point reply to both reviews. The text from the reviews is highlighted by italics.

1.1 Review #1

We like to thank Richard Wilson for reviewing our manuscript and express our gratitude for his suggestions. A point-by-point answer to his comments is given in the following.

The article "Evaluation of wake influence on high-resolution balloon-sonde measurements" addresses the possible impact of the wake-created fluctuations on turbulence measurements from rising balloons. Such a wake can be generated in the trail of the balloon and/or by objects in the vicinity of the sensors (gondola, rope). The authors show few examples of likely wake encounter based on very high-resolution (8 kHz) measurements of the wind velocity from their LITOS instrument. These examples are convincing as they show large velocity fluctuations hardly distinguishable from atmospheric turbulence when the payload is likely in the balloon wake. The approach of this work is mostly probabilistic, the main aim is to estimate the probability for wake encounter by the payload hanged below a rising balloon. Based on a probabilistic model, the authors estimate the relative impact of various factors, some of them not being considered in previous works such as the vertical wind or the rotation of the wind vector. As expected, the probability for the payload to be in the wake depends mainly on the balloon-gondola distance and on the vertical shear of the horizontal wind. From a statistical study based on 30 radiosondes, they estimated the probability for the payload to be in the wake of the balloon. They concluded that the probability for such an encounter for standard radiosondes is 28% in the average. The article addresses a relevant question: to what extent does the disturbances induced by the system carrying a high resolution sensor impact turbulence measurement? The authors convincingly show (1) some effects of such disturbances (2) that the probability for the payload to be in the wake is quite large even for large balloon-payload distances, and (3) that this issue must be carefully addressed when estimating atmospheric turbulence from instruments carried by rising balloons. The possible wake effects are obvious for high-resolution sensors, but may also impact turbulence detections from standard resolution (1 Hz) radiosondes.
Undoubtedly, this article deserves to be published. It is well organized, well written (as far as I can judge). The figures are appropriate and well made. The quotes seem relevant to me. I generally appreciated this work.

We are grateful for this kind assessment of our article.

1) I wonder about the possible impact of wake on the turbulence detection from standard radiosondes. This issue could be addressed by considering the statistics of the time during which the payload stays in the wake, i.e. of the spatial extent of the payload-wake encounters. The two presented example have spatial extent of 15 m and 6 m, hardly detectable from radiosonde measurements (some authors - Ferron et al., Wilson et al. - recommend to undersample the vertical profile in order to detect inversions in the potential temperature profile. For radiosondes, this lead to vertical resolution of about 15 m). Do the authors think that such a statistics could be obtained from the presented probabilistic model? Perhaps beyond the subject of the paper, I think such a result could increase the scope of this work.

We clearly share the opinion that retrieving the proposed statistics would increase the scope of this work. Unfortunately however, we do not see a way forward to obtain the necessary information. This is the case for two reasons:

- Retrieving the statistics from our LITOS measurement does not work, because the wake from the ropes partly masks the wake from the balloon thereby introducing a bias towards smaller spatial extends of the payload-wake encounters.

- Retrieving the statistics purely from our wake detection algorithm might be questionable, because the wake encounter probability does not give a clear discrimination between wake affected and wake free altitude bins. We chose to discard all turbulence measurements from altitude bins showing $P_{\text{wake}} > 5\,\%$ in order to avoid wake influence on our turbulence measurements. Retrieving such statistics using the 5 % threshold however, would overestimate the spatial extend of the payload-wake encounters.

Nevertheless, we still assume that these wake encounters may influence Thorpe analyses from standard radiosondes even if the dataset is undersampled to a vertical resolution of about 15 m. Tiefenau and Gebbeken (1989) find periods of 5.5 s and 11 s on radiosonde temperature data caused by the payload swinging in and out of the balloon's wake. We assume that such long periods may be detectable even in undersampled radiosonde data sets.

2) p17, l5-6: Can you be more specific about this affirmation?

In order to solidify this affirmation, we added a visualization of the ninety-fifth percentile of the radiosonde dataset to the plots of this section. Furthermore, we calculated the spread of the wake probability depending on changes in wind shear, rotation of the wind vector and changes in relative vertical velocity, respectively. The revised text reads: "From the analysis of these three parameters, we find that within the ninety-fifth percentile of the wind shear for the given radiosonde dataset, the wake probability changes from 0.1 % to 96 %. Within the ninety-fifth percentile of all examined rotations in the horizontal wind vector the wake probability changes from 68 % to 95 %. For the variation in relative vertical balloon velocity the wake probability changes from 43 % to 84 %. Therefore, we conclude that within the spread of the given radiosonde dataset wind shear has the strongest influence on the likelihood for wake encounter."

3) p21, l15-16: the assertion that the wake of the balloon contributes to noise (meaning instrumental noise) is questionable. The signatures of the balloon's wake on the temperature profile, either temperature peaks or turbulent eddies, are not a contribution to instrumental noise (assumed uncorrelated), but are likely responsible of false inversions in the potential temperature profile.

We agree with the reviewer that our assumption resulted from misinterpreting the role of instrumental noise in Wilson et al. (2010) and Wilson et al. (2011). The corresponding statements have been deleted from our discussion.

Minor comments

p8, l13: Euklidian -> Euclidian

Thanks for pointing out this typo. The correction has been made.

p 8, l10: why a factor 2 in the definition of L?

The factor of two in the definition of L is a safety margin. It is needed, because in case the wind shear changes over the distance between the payload and the balloon the

wake will not move along a straight line and will therefore need more timesteps to reach the closest distance to the payload. However, we agree that a factor of 2 is excessive for this purpose. In order to save computational cost, this factor has been reduced to 1.2 in the revised manuscript.

p8, l10: the notation L = (...). min(w_rel) is not very satisfactory (the dot can be read as an operator...)

Thanks for the suggestion. We changed the sentence to " L = (...). In this case, min(w_rel)".

Appendix and figure A1: Can one conclude that w is estimated to be zero in the troposphere for all flights?

We cannot sensibly estimate w in the troposphere due to aerodynamically induced variations in the ascent rate. Our wake prediction algorithm however needs an input for w. Therefore, we set $w = 0$ in the critical and supercritical Reynolds number range. To make this more visible, we replaced the solid line in Figure A1 by a dotted line where w is set to zero.

1.2 Review #2

We are grateful for the effort undertaken by the reviewer and like to thank her/him for the constructive recommendations. A point-by-point answer is given below.

This manuscript provides a comprehensive analysis of wake effects on balloon-borne measurements. The analysis is focused on highly sophisticated turbulence measurements of the LITOS project but provides also important information for other balloon experiments. The analysis is sound, and the manuscript is well written and very suited for publication in AMT. I recommend publication after a minor revision. My comments mainly concern clarifications that probably would make the paper more accessible/useful to a broader audience.

We are thankful for the positive feedback from the reviewer. We hope that our changes will increase the accessibility of our manuscript.

What is actually a typical wake effect on measurements of turbulence (or other quantities like temperature or humidity)? Please provide more information about this to the unexperienced reader.

Thanks very much for your suggestion. We have added the following paragraph to the introduction that highlights the impact of wake created turbulence.
"On measurements of turbulent velocity fluctuations, the wake from the balloon can hardly be distinguished from atmospheric turbulence of the same strength. With our LITOS instrument we found that the spectral shape of the velocity fluctuations does not allow a distinction between atmospheric turbulence and wake. Depending on the payload-balloon distance, we found dissipation rates created by the balloon's wake between $10^{-4}\,W\,kg^{-1}$ and $10^{-2}\,W\,kg^{-1}$. In terms of aviation turbulence categories, these dissipation rates correspond to "light" and "moderate" turbulence using the scaling of Sharman et al. (2014) for medium-sized aircraft. Wake effects from the ropes holding the gondola show consistently "severe" turbulence intensities around $10^{-1}\,W\,kg^{-1}$. Accordingly, these effects should not be neglected for turbulence measurements from rising balloons. For standard radiosondes Kräuchi et al. (2016) report a warm bias of 1 K on average for a daytime sounding in the stratosphere. Furthermore, moisture from the balloon's skin will lead to a wet bias of stratospheric humidity if the sensor is in the balloon's wake."

The manuscript seems to provide examples both of increased turbulence and decreased turbulence in the wake (figure 3; page 11, line 5-9; page 11, line 12-13).

According to our understanding, the strength of wake related turbulence depends on the payload-balloon distance and possibly on the size of the balloon or the ascent rate. We found kinetic energy dissipation rates from $10^{-4}\,W\,kg^{-1}$ to $10^{-2}\,W\,kg^{-1}$. This, however, is not related to the strength of atmospheric turbulence. Therefore, atmospheric turbulence may be weaker as well as stronger than wake related turbulence. In order to point this out, we changed the paragraph following page 11, line 7:
"We like to stress, however, that the data underlying Figure 1 show only one exemplary case of a turbulent altitude bin. Under different atmospheric conditions, LITOS measured atmospheric turbulence ranging from $0.001\,mW\,kg^{-1}$ to $100\,mW\,kg^{-1}$. In contrast, we typically find dissipation rates between $0.01\,mW\,kg^{-1}$ and $1\,mW\,kg^{-1}$ for balloon-wake induced turbulence. However, during previous measurements with lower payload-balloon distances we measured wake induced turbulence stronger than $10\,mW\,kg^{-1}$ (data not

shown here)."

At several places in the manuscript it is stated that the wake does not have a clear outer boundary. Rather, one would expect, a continuous transition from a perturbed region to an unperturbed region. On the other hand you use the notation "inside the wake" and "outside the wake" throughout the manuscript. And you introduce e.g. the "radius of the wake" (page 10, line 11). This is not consistent and should be clarified.

We are sorry for our inconsistent terminology on this matter. To our understanding, there is a clear outer boundary of the wake. However, the transversal distance of the outer boundary of the wake to the wake's centre will change depending on the downstream distance from the balloon. This is, because the outer boundary of the wake is shaped by larger eddies. A visualisation of the flow in a turbulent wake showing a fairly clear outer boundary is given in Jang and Lee (2008, Figure 11b). Even though we expect a clear outer boundary, we cannot state its distance from the wake centre for a given downstream distance to the balloon due to the chaotic flow in the wake. This is one of the main reasons to take a probabilistic approach in our wake detection algorithm. The sentence on page 3, lines 3-7 has been changed to:
"Furthermore, we consider that the diameter of the balloon's wake changes on short time scales of a few seconds due to the production of larger vortices. Furthermore, its mean diameter increases on longer timescales in the order of several 10 seconds. Since the balloon's contour resembles a sphere during flight, we can refer to fundamental experiments done in wind tunnels (e.g. Riddhagni et al., 1971; Gibson and Lin, 1968). An informative visualisation of such a flow can be found in Jang and Lee (2008, Figure 11)."
Furthermore, page 7, line 5 has been amended. It reads:
"Due to the intermittent nature of the turbulent wake, its diameter changes on downstream length scales smaller than a few balloon diameters."

Most analysis in the paper is done in terms of likelihood for instruments to encounter the wake of the balloon (or of the payload chain). What would desirable for balloon researchers is a more "deterministic" algorithm that provides a rather clear statement Yes or No about being influenced by a wake effects in a given situation. Do the authors see any way forward towards developing such a "deterministic" analysis tool?

We fully agree with the reviewer that a deterministic tool to determine whether the balloon's gondola is inside or outside the wake would be highly desirable. Unfortunately however, we do not see a way to create such a tool using radiosonde wind data. The main reason for this conclusion is that the uncertainty in the payload-wake distance ($\Delta_{d_{\mathrm{p-wake}}}$) is in the same order of magnitude as the payload-wake distance ($d_{\mathrm{p-wake}}$). From our point of view this requires an uncertainty analysis, which is done in our probabilistic approach. The uncertainty in the position of the balloon ($\Delta_{X_{\mathrm{p-wake}}}$) could only be reduced by using an additional GPS receiver attached to the balloon. The uncertainties in the radiosonde wind measurement (Δ_U) and in the payload position ($\Delta_{X_{\mathrm{p}}}$) however, could be generally reduced by enhancing precision and sampling rate of the radiosonde. Nevertheless, these measures would still not remove the uncertainty in the diameter of the wake (as discussed in the previous point). In conclusion, one could reduce the uncertainties in the calculation with a high technical effort, but would still not be able to fully avoid a probabilistic approach. Therefore, we assume that our approach provides a

helpful compromise between usability and certainty in the prediction.

On page 11, line 12-13, you refer to probabilities exceeding 95% as "wake affected within uncertainty". Would you not consider significantly lower probabilities (e.g. 80% or 60%) as being "wake affected within uncertainty". What is the significance of the number 95%?

Our aim is to sort out all data bins that are not most certainly wake free. Therefore, we only use turbulence measurements from altitude bins showing $P_{\text{wake}} < 5\,\%$. From our point of view a significantly lower confidence level (accepting turbulence measurements with $P_{\text{wake}} \gg 5\,\%$ would illicitly increase the risk of misinterpreting wake created turbulence for atmospheric turbulence. Accordingly, we define altitude bins with a wake probability above 95 % as wake affected in order to be consistent with our definition of wake free altitude bins. To make our wording more precise, we removed "within uncertainty" from page 11, line 13 of the manuscript.

Related to the above questions: On page 4, line 18, you refer to a measurement unperturbed by ant wake effect. How do you know this?

We know that there are no wake effects on this measurement, because we measured on a descending balloon with our sensors pointing downward. Accordingly, all parts of the payload are located downstream of our sensors. Therefore, the sensors cannot be hit by the wake from these objects.

It would be instructive if you in your conclusions formulated some general advice for balloon researcher about how to deal with wake effects.

Thank you very much for pointing this out. We added the following sentence to our conclusion:
"For research purposes where the complete avoidance of any wake influence is crucial (e.g. turbulence measurements, high accuracy temperature soundings), we strongly recommend to measure on a descending balloon with the sensor pointing downward."

<u>Some minor comment:</u> Om page 3, lines 9, 12, 15: It is unclear what "their" refers to in this paragraph. It somehow refers to "other studies" in line 8. Please clarify the formulations.

Thanks for identifying this issue. We changed the sentences to:
"The most common method to obtain energy dissipation rates from radiosonde temperature profile has been adapted from oceanic sciences by Luce et al. (2002) and Clayson and Kantha (2008). It is frequently referred to as the "Thorpe analysis." Energy dissipation rates are inferred from the vertical displacement (Thorpe displacement) of an air parcel compared to a statically stable profile (Wilson et al., 2010, 2011). Typically, for a standard radiosonde the distance between the balloon and the sensor is between 30 m and 55 m. This makes the measurements susceptible to distortions from the balloon's wake (e.g. Jumper and Murphy, 2001; Kräuchi et al., 2016). Hence, our wake evaluation tool may be used to assess the likelihood of wake influence for every altitude bin of a Thorpe analysis turbulence retrieval, depending on the balloon-payload distance of the instrument."

On page 9, line 9-12, you introduce the amplitude of the balloons horizontal motion. It would be instructive to provide the reader with some typical numbers for this amplitude, e.g. for the LITOS case.

We have added the following statement to the text: "Typically, D_{bal} is below 10 m.

In the case of the LITOS launch from 29 January 2016 (discussed in Section 3.1.4) the mean amplitude in the critical and supercrititcal Reynolds number range is 6.3 m."

2 Further changes to the manuscript

In the following, we list all relevant changes to the manuscript that are not related to the reviews.

- p. 4, l .16:
  "The geometric mean of the dissipation rate from both sensors is $9.9\,\mathrm{mW\,kg^{-1}}$, which corresponds to a moderate turbulence intensity according to aviation standards (Sharman and Pearson, 2017)." $\rightarrow$ "The geometric mean of the dissipation rate from both sensors is $9.9\,\mathrm{mW\,kg^{-1}}$, which corresponds to a moderate turbulence intensity for medium-sized aircraft according to aviation standards (Sharman et al., 2014)."

- p.8, l. 15:
  $d_{\text{p-wake}}(t^l) = |\vec{X}_p(t^l) - \vec{X_{\text{wake}}}(t^l)| \rightarrow$
  $d_{\text{p-wake}}(t^l) = \min_{m=0,\ldots,L} |\vec{X}_p(t^l) - \vec{X_{\text{wake}}}(t^l)|$

3 Marked-up manuscript

Evaluation of wake influence on high-resolution balloon-sonde measurements

Jens Söder[1], Michael Gerding[1], Andreas Schneider[1,a], Andreas Dörnbrack[2], Henrike Wilms[2], Johannes Wagner[2], and Franz-Josef Lübken[1]

[1]Leibniz Institute of Atmospheric Physics at the University of Rostock (IAP), Kühlungsborn, Germany
[2]German Aerospace Center (DLR), Institute of Atmospheric Physics (IPA), Wessling, Germany
[a]now at: SRON Netherlands Institute for Space Research, Utrecht, the Netherlands

Correspondence to: Jens Söder (soeder@iap-kborn.de)

Abstract. Balloons are used for various in-situ measurements in the atmosphere. On turbulence measurements from rising balloons there is a potential for misinterpreting wake-created fluctuations in the trail of the balloon for atmospheric turbulence. These wake effects have an influence on temperature and humidity measurements from radiosondes as well. The primary aim of this study is to assess the likelihood for wake encounter on the payload below a rising balloon. Therefore, we present a tool for calculating this probability based on radiosonde wind data. This includes a retrieval of vertical winds from the radiosonde and an uncertainty analysis of the wake assessment. Our wake evaluation tool may be used for any balloon-gondola distance and provides a significant refinement compared to existing assessments.

We have analysed wake effects for various balloon-gondola distances applying atmospheric background conditions from a set of 30 radiosondes. For a standard radiosonde we find an average probability for wake encounter of 28 %, pointing out the importance of estimating wake effects on sounding balloons. Furthermore, we find that even millimetre sized objects in the payload can have significant effects on high-resolution turbulence measurements, if they are located upstream of the turbulence sensor.

1 Introduction

Since their advent in the beginning of the 20th century (e.g. Aßmann, 1902) rubber-made sounding balloons provide a major platform for atmospheric in-situ soundings of wind, temperature and humidity. To the present day, radiosondes are routinely used for the assimilation of numerical weather predictions (e.g. Bouttier and Kelly, 2001). These balloons are approximately spherically shaped during flight. Horizontally, they drift with the atmospheric wind. Vertically, they rise with a speed of about $5\,\mathrm{m\,s^{-1}}$ relative to the atmosphere. This rise creates a turbulent wake downstream (below) of the balloon (e.g. Taneda, 1978). It mainly depends on the wind-shear in the atmosphere, whether the balloon's wake will hit the sensors on the payload or not. Therefore, great care has to be taken when interpreting turbulence measurements from rising balloons, because they may be influenced by the balloon's wake (Barat et al., 1984). Furthermore, other studies showed an influence of the wake on temperature and humidity measurements from standard radiosondes as well (Tiefenau and Gebbeken, 1989; Gaffen, 1994;

Kräuchi et al., 2016). Wakes can also be generated by other parts of the payload, e.g. ropes holding the gondola. We refer to these objects as the "payload chain".

In the first place, our interest into the subject was triggered because we wanted to improve the data quality on our balloon-borne LITOS instrument (Leibniz-Institute Turbulence Observations in the Stratosphere, Theuerkauf et al., 2011; Schneider et al., 2017). LITOS uses a Constant Temperature Anemometer (CTA) to investigate the Power Spectral Density (PSD) of turbulent velocity fluctuations down to spatial scales of centimetres. This enables us to resolve the transition from the inertial to the viscous subrange of turbulence. We use this approach to retrieve atmospheric energy dissipation rates. Horizontal winds are acquired from a standard radiosonde on the same balloon. ~~However, LITOS is sensitive enough so that the measurements can be seriously flawed if the payload is hit~~

On measurements of turbulent velocity fluctuations, the wake from the balloon can hardly be distinguished from atmospheric turbulence of the same strength. With our LITOS instrument we found that the spectral shape of the velocity fluctuations does not allow a distinction between atmospheric turbulence and wake. Depending on the payload-balloon distance, we found dissipation rates created by the balloon's wake ~~, even though the sensor is located 180~~between $10^{-4}\,\mathrm{W\,kg^{-1}}$ and $10^{-2}\,\mathrm{W\,kg^{-1}}$. In terms of aviation turbulence categories, these dissipation rates correspond to "light" and "moderate" turbulence using the scaling of Sharman et al. (2014) for medium-sized aircraft. Wake effects from the ropes holding the gondola show consistently "severe" turbulence intensities around $\sim 10^{-1}\,\mathrm{W\,kg^{-1}}$. Accordingly, these effects should not be neglected for turbulence measurements from rising balloons. For standard radiosondes, Kräuchi et al. (2016) report a warm bias of 1 K ~~below the balloon. This is also the case for velocity fluctuations related to the wake of the ropes holding the main gondola~~on average for a daytime sounding in the stratosphere. Furthermore, moisture from the balloon's skin will lead to a wet bias of stratospheric humidity if the sensor is in the balloon's wake.

Therefore, our question in this study is: Can we determine from a radiosonde measurement, in which altitude the instrument was exposed to turbulence generated from the balloon or from smaller objects in the payload chain?

Pioneering work with regard to the influence of the balloon's wake on turbulence measurements has been done by Barat et al. (1984). They calculated the distance between the wake's centre and the gondola from the wind shear measured with their instrument. They concluded that every altitude bin of their measurement is wake free, where the distance between the wake's centre and the gondola is larger than two balloon diameter. However, they did not consider uncertainties in their wind shear measurement and did not directly include other findings showing that the wake of a spherical body does not have sharp boundaries but is rather fringed at the edges (e.g. Riddhagni et al., 1971). Furthermore, they did not consider vertical winds in their approach. We take those effects into account and refine their technique by applying a probabilistic approach.

The general idea behind our wake evaluation tool is to calculate the advection of the balloon's wake using a radiosonde wind measurement from the same balloon. For every time step, the minimal distance between the wake's centre and the payload is calculated. This concept is similar to the one used by Barat et al. (1984). In contrast however, we take into account the uncertainty in that calculation. Therefore, it is important to consider self-induced motions of the balloon due to changing aerodynamic forces in the critical and supercritical Reynolds number range, because they influence the wind measurement of the radiosonde. Murrow and Henry (1965) conducted tests within a large hangar, whereas MacCready (1965) and Scoggins

(1965) examined outdoor launches in still air. A comprehensive review on wind measurements using sounding balloons is given by Scoggins (1967). We use their results in our study to obtain estimates for the magnitude of those self-induced motions observed on sounding balloons.

Furthermore, we consider that the diameter of the balloon's wake ~~does not have a sharp outer boundary and that its diameter increases with time~~changes on short time scales of a few seconds due to the production of larger vortices. Furthermore, its mean diameter increases on longer timescales in the order of several 10 seconds. Since the balloon's contour resembles a sphere during flight, we can refer to fundamental experiments done in wind tunnels (e.g. Riddhagni et al., 1971; Gibson and Lin, 1968). An informative visualisation of such a flow can be found in Jang and Lee (2008, Figure 11). More recently, numerical simulations of flows at relevant Reynolds numbers have become available. For example Dommermuth et al. (2002) examined the width of the wake of a sphere in stratified and non-stratified fluids using Large-Eddy-Simulations. They mainly confirm the results of previous laboratory studies.

Additionally, we modify the approach from Barat et al. (1984) by considering vertical winds in our wake evaluation tool. Earlier vertical wind retrievals assumed that all major fluctuations in the ascent rate are comparable to vertical wind fluctuations by gravity waves (e.g. Shutts et al., 1988; Lalas and Einaudi, 1980). Reeder et al. (1999) and Gong and Geller (2010), respectively, subtract a running mean or a second order polynomial from the ascent rate to retrieve vertical winds. Wang et al. (2009) as well as Gallice et al. (2011) extend these approaches by modelling the ascent of the balloon based on a physical description of the relevant forces. In this work, we present and use a modified version of the Wang et al. (2009) model.

With this new approach, we can calculate the likelihood for encountering the balloon's wake using a radiosonde wind profile. Besides its importance for specially designed turbulence sensors like LITOS, it may be of interest for other studies retrieving turbulent energy dissipation rates from standard radiosondes. ~~Their method~~ The most common method to obtain energy dissipation rates from radiosonde temperature profiles has been adapted from oceanic sciences by Luce et al. (2002) and Clayson and Kantha (2008). It is frequently referred to as the "Thorpe analysis". Energy dissipation rates are inferred from the vertical displacement (Thorpe displacement) of an air parcel compared to a statically stable profile (Wilson et al., 2010, 2011). Typically, ~~their~~ for a standard radiosonde the distance between the balloon and the sensor is between 30 m and 55 m. This makes the ~~measurements~~ measurement susceptible to distortions from the balloon's wake (e.g. Jumper and Murphy, 2001; Kräuchi et al., 2016). Hence, our wake evaluation tool may be used to assess the likelihood of wake influence for every altitude bin of ~~their turbulence measurement~~a Thorpe analysis turbulence retrieval, depending on ~~their~~ the balloon-payload distance of the instrument.

Even for longer balloon-payload distances, we cannot expect the balloon's wake to dissolve before it encounters the sensor. Kyrazis et al. (2009) found from a review of laboratory experiments that the wake persists up to 1000 diameters downstream of the balloon.

In the following, we give a short overview on our turbulence evaluation scheme (Section 2). In Section 3, a tool for calculating the likelihood of wake encounter at the payload position is presented. This includes applying the tool to a set of 30 radiosonde launches. Influences of wake caused by the payload chain are shown in Section 4 and results are discussed in Section 5. In Appendix A the retrieval of vertical winds from a standard radiosonde is presented.

2 Retrieving Energy dissipation rates from wind fluctuation data

In order to infer energy dissipation rates, LITOS measures wind fluctuations with two constant temperature anemometers (CTAs) at a frequency of 8 kHz. The handling of these data is explained in this section. Further atmospheric quantities are measured with a radiosonde (Väisälä RS-41: for details please see Survo et al., 2014) and the pendulum motion of the gondola below the balloon is calculated from an inertial sensor (ADIS16407 by Analog Devices, mounted on the LITOS gondola). For measurements in the ascent phase, the LITOS gondola is typically located 180 m below the balloon (radiosonde: 235 m below the balloon). Details of the current LITOS instrument have been described by Schneider et al. (2017).

To retrieve atmospheric turbulence we divide our CTA data into time bins of 10 s, calculate the power spectral density (PSD) for each bin and fit the Heisenberg (1948) spectrum of turbulence to the data. In this paper, we will only give a brief overview on retrieving energy dissipation rates, further details can be found in Schneider (2015) and Schneider et al. (2017). For the fit, we use an adaption of the Heisenberg function to velocity fluctuations as a function of angular frequencies ω given by Schneider (2015, Eq. A.56) based on the idea presented in Lübken (1992):

$$W(\omega) = C_\mathrm{v}^2 \frac{\Gamma\left(\frac{5}{3}\right)\sin\left(\frac{\pi}{3}\right)}{2\pi w_\mathrm{rel}} \frac{(\omega/w_\mathrm{rel})^{-5/3}}{\left(1+\left(\frac{\omega}{\omega_0}\right)^{8/3}\right)^2}. \tag{1}$$

The structure function constant C_v and the angular frequency $\omega_0 = \frac{2\pi w_\mathrm{rel}}{l_0}$ (representative of the inner scale l_0) are used as fit parameters. Γ denotes the gamma function, and w_rel is the relative vertical velocity between the sensor and the atmosphere. It is calculated from the ascent rate of the balloon w_asc and the vertical wind w:

$$w_\mathrm{rel} = w_\mathrm{asc} - w. \tag{2}$$

Our method for retrieving vertical winds from radiosonde data is explained in Appendix A. Generally, we infer energy dissipation rates ϵ from the inner scale l_0 according to Schneider (2015, Eq. A.48):

$$\epsilon = c_{l0}^4 \frac{\nu^3}{l_0^4}. \tag{3}$$

c_{l0} is a constant depending on the sensor orientation (in our case: $c_{l0} = 15.8028$; Schneider et al., 2017). ν denotes the kinematic viscosity and is calculated from radiosonde temperatures T and densities ρ (c.f. NOAA, 1976):

$$\nu = \frac{1.458 \cdot 10^{-6} \cdot T^{3/2}}{\rho(T + 110.4)}. \tag{4}$$

Exemplary spectra of velocity fluctuations are given in Figure 1 together with a plot of the fit function (Eq. 1). We find that the fit function generally follows the measured data considering the noise of the PSD. The inner scale l_0 is $\sim 2.5\,\mathrm{cm}$, underlining the need for high-resolution measurements. The geometric mean of the dissipation rate from both sensors is $9.9\,\mathrm{mW\,kg^{-1}}$, which corresponds to a moderate turbulence intensity for medium-sized aircraft according to aviation standards ~~(Sharman and Pearson, 2017)~~(Sharman et al., 2014). The data presented in Figure 1 are taken on a descending balloon. The sensors were located below the gondola, measuring the atmospheric flow unperturbed by any wake effects.

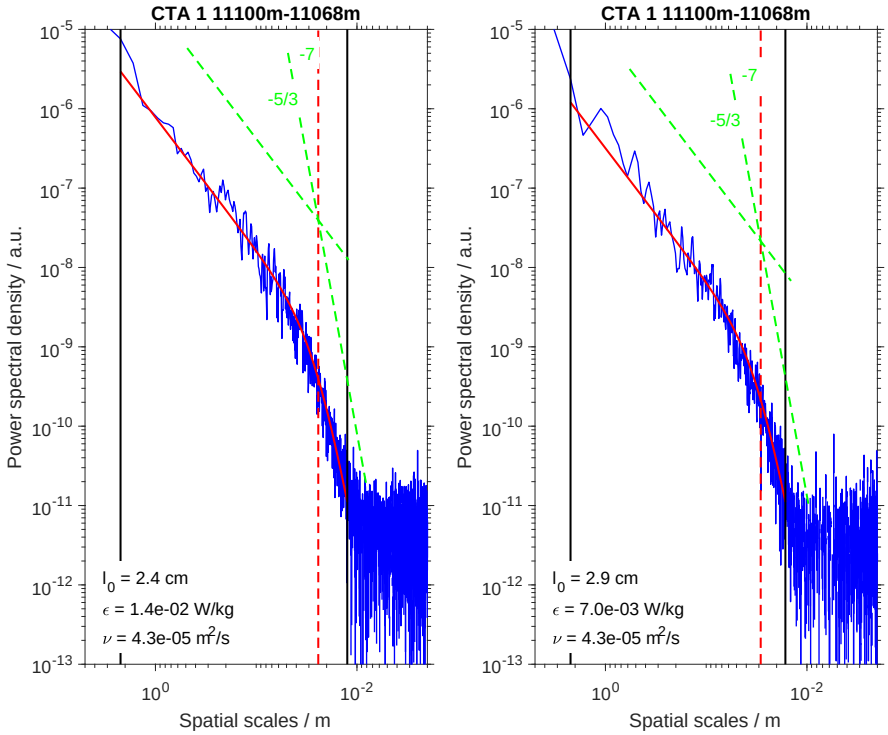

Figure 1. Power spectral densities of undisturbed atmospheric turbulent velocity fluctuations (dark blue). The spectra show data from two independent CTA measurements on the same gondola in the same 10 s time span on a descending balloon (06 August 2016). The solid red curve gives the fit of Heisenberg's turbulence model. The transition between the inertial (-5/3) and the viscous (-7) subrange is given by the vertical dashed red line (inner scale l_0). Vertical black lines: fit range. Energy dissipation rates ϵ and kinematic viscosities ν are given in the lower left corner of each panel.

3 Wake caused by the balloon

In this section we describe a "wake evaluation tool" to calculate the likelihood of a wake encounter of the gondola below a rising balloon. Generally, all distances are denoted by a lower-case "d", all diameters by an upper-case "D" and all radii by an upper-case "R". For additional information on the source code please see Section 7. Further below we statistically evaluate a series of 30 radiosonde launches and inspect the influence of wind shear, rotation of the horizontal wind vector, relative vertical velocity and balloon-payload distance by using artificial data.

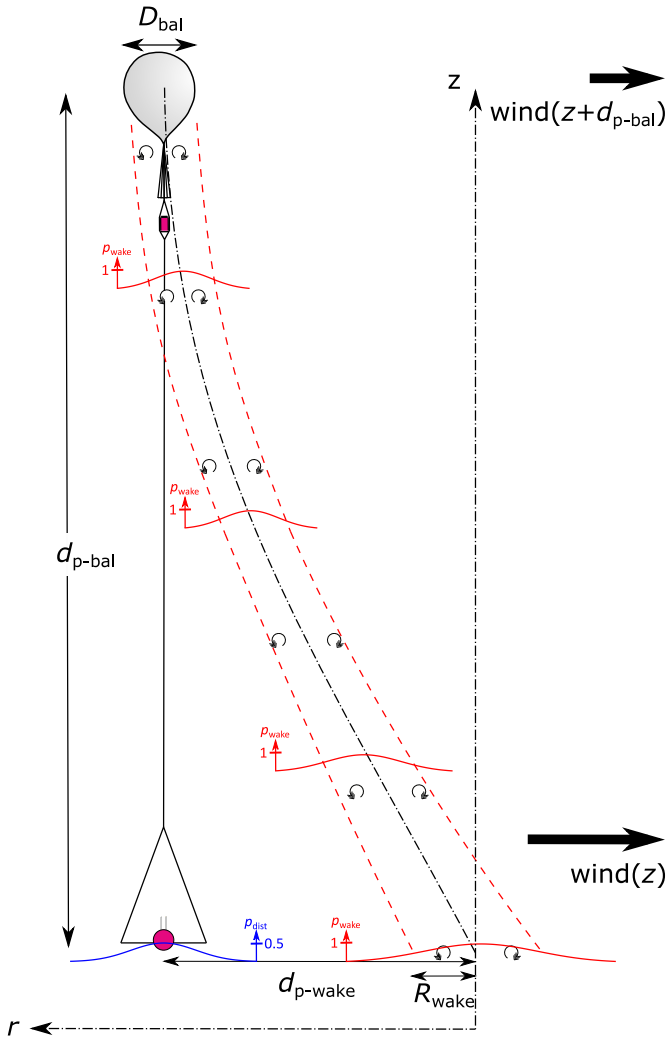

Figure 2. Flow within the LITOS payload chain. $d_{\text{p-bal}}$: distance between the payload and the centre of the balloon. $d_{\text{p-wake}}$: distance between the centre of the balloon's wake and the payload. Red lines: distribution of the probability for being in the wake (dashed red line showing the FHWM). Blue line: probability distribution for the payload-wake distance $d_{\text{p-wake}}$. Sketch is not to scale, the radiosonde below the LITOS gondola is omitted for clarity.

3.1 Method

3.1.1 Payload-wake distance

The concept of our wake evaluation tool is that for every timestep of the calculation, a spherically shaped wake is created from the position of the balloon centre. Each wake is advected with the wind. I.e. the wake does not move, if the fluid is at rest,

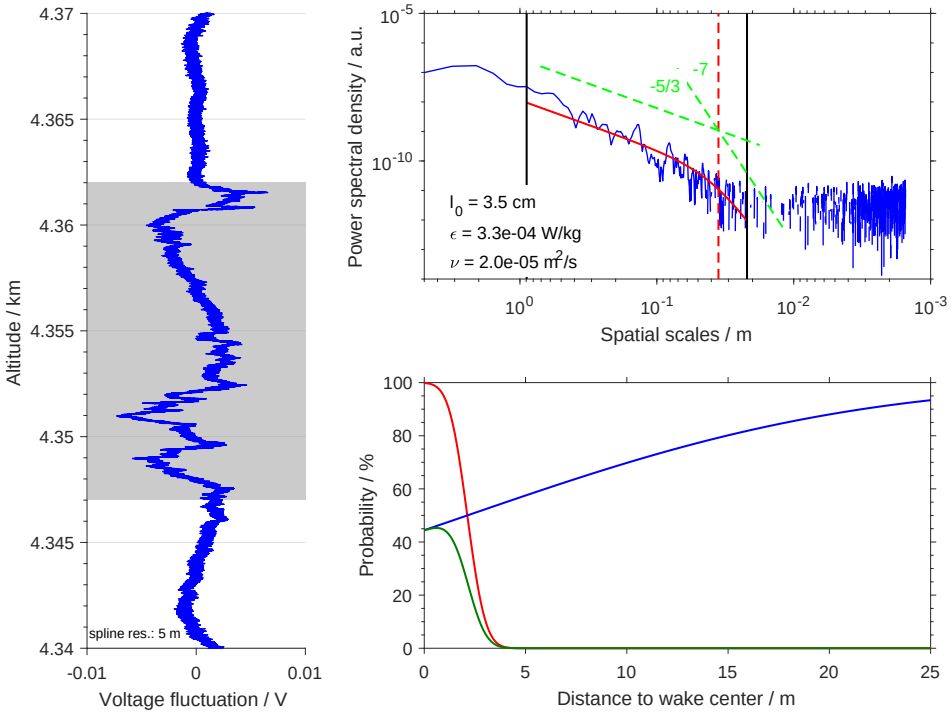

Figure 3. Example for turbulence caused by the balloon's wake from a LITOS launch on 29 Jan 2016. Left: Raw data from the CTA, grey shaded area influenced by wake. Top right: Turbulence retrieval fit as in Figure 1 from the data shown in the shaded area. Bottom right: Result from the wake prediction algorithm for the same altitude. Blue: Probability distribution of the payload-wake distance $d_{\text{p-wake}}$ to be in the range of $[0, d]$ after Equation 12. Red: Radial probability distribution of the wake after Equation 13. Green: Combined probability for wake encounter P_{wake} according to Equation 16 .

but is advected horizontally and vertically with the wind. A sketch of the flow within the LITOS payload chain is given in Figure 2. Please note that the depicted path of the wake depends on the wind shear between the balloon and the payload as well as on the relative vertical velocity of the balloon w_{rel}, but not on the magnitude of the wind speed. In order to get the distance between the wake centre and the payload, $d_{\text{p-wake}}$, we look for the closest distance at a specific time between the payload and all created wakes. Due to the intermittent nature of the turbulent wake, ~~it has no clear outer boundary~~its diameter changes on downstream length scales smaller than a few balloon diameters. Therefore, we determine the probability for being in the wake at a certain distance to the wake centre. Furthermore, there is an uncertainty on the calculated payload-wake distance $d_{\text{p-wake}}$ due to measurement errors, which is included in our probabilistic approach. This probability for encountering the balloon's wake at the payload position increases for small balloon-payload distances $d_{\text{p-bal}}$ and low wind shears.

The retrieval of $d_{\text{p-wake}}$ is done using radiosonde wind data that have been low-pass filtered with a cut-off frequency of 1/40 Hz to avoid the influence of self-induced balloon motions on the wind estimate (e.g. MacCready, 1965). For this we use a third order digital Butterworth filter. The position of the payload at the time $t^n = k\tau$ with timestep τ and $k = 0, 1, 2, ..., n$ may be written as:

$$\boldsymbol{X_p}(t^n) = \boldsymbol{X_0} + \sum_{k=0}^{n} \begin{pmatrix} u(t^k) \\ v(t^k) \\ w_{\text{asc}}(t^k) \end{pmatrix} \tau, \tag{5}$$

with $\boldsymbol{X_0}$ being the launch position and u, v, the horizontal wind components measured by the radiosonde. This equation is valid under the assumption that the combined aerodynamic centre of the balloon and the payload chain is close to the midpoint of the balloon. Therefore, especially for longer payload-balloon distances radiosonde wind data need to be shifted in altitude in order to account for this effect. Furthermore, we expect the payload chain to be hanging straight below the balloon. Any pendulum motions of the gondola are handled as described in Section 3.1.2.

The radiosonde data are given at a rate of 1 Hz. For an average ascent rate of $5\,\mathrm{m\,s^{-1}}$, this results in a vertical distance of the data points of 5 m, which is in the same order of magnitude as typical payload-wake distances $d_{\text{p-wake}}$ especially for short payload-balloon distances $d_{\text{p-bal}}$ below 100 m. In order to avoid large errors on the payload-wake distance due to this coarse gridding, we linearly interpolate the radiosonde data to a timestep $\tau = 1/5\,\mathrm{s}$.

For each time t^n, there will be a wake created at the position of the balloon $\boldsymbol{X_{\text{bal}}}(t^n)$, which is located $d_{\text{p-bal}}$ above $\boldsymbol{X_p}(t^n)$. We assume the position of the centre of that particular wake $\boldsymbol{X_{\text{wake}}}(t^m)$ to be moving with the wind taken at the previous balloon position at time t^n. This means that the balloon's wake moves with the background wind that is measured at time t^n. In other words, we assume this background wind to be constant for the time it takes to lift the payload through the payload-balloon distance:

$$\boldsymbol{X_{\text{wake}}}(t^l) = \boldsymbol{X_{\text{bal}}}(t^n) + m \begin{pmatrix} u(t^n) \\ v(t^n) \\ w(t^n) \end{pmatrix} \tau, \tag{6}$$

with $t^l = t^n + m\tau$, $m = 0, 1, 2, ..., L$ and ~~$L = \left(\frac{2 d_{\text{p-bal}}}{\min(w_{\text{rel}})\tau}\right)$~~. $L = \left(\frac{C_{\text{sh}}\, d_{\text{p-bal}}}{\min(w_{\text{rel}})\tau}\right)$. In this case, $\min(w_{\text{rel}})$ denotes the minimal relative ascent rate during the whole flight (c.f. Appendix A). L is an estimate for the maximum number of timesteps the payload needs to fly through the payload-balloon distance. It is introduced in order to save computational power and does not have a physical meaning in terms of the wake's life time. The constant $C_{\text{sh}} = 1.2$ accounts for a possible change in wind shear that would increase the number of timesteps until the wake reaches its closest position to the payload. For each time t^l, we calculate the minimal ~~Euklidian~~ Euclidian distance between the LITOS gondola and the wake centre:

$$d_{\text{p-wake}}(t^l) = \min_{m=0,...,L} |\boldsymbol{X_p}(t^l) - \boldsymbol{X_{\text{wake}}}(t^l)|. \tag{7}$$

An example for an altitude range of our LITOS data affected by the balloon's wake is shown in Figure 3.

3.1.2 Uncertainty in the payload-wake distance

Due to measurement errors of the radiosonde and self-induced motions of the balloon caused by aerodynamic forces, there is an uncertainty on the payload-wake distance $d_{\text{p-wake}}$. It will be governed by three main components: the uncertainty in the wind measurement Δ_U, the uncertainty in the position of the payload Δ_{X_p}, and the uncertainty in the position of the balloon. Δ_U consists of the uncertainty of the vertical wind retrieval and the uncertainty of the radiosonde measurement (resulting from the uncertainty in the GPS position). The error in the vertical wind Δ_w is assumed to be $2\,\text{m}\,\text{s}^{-1}$ below 19.5 km altitude and $1\,\text{m}\,\text{s}^{-1}$ above (c.f. Appendix A). Below 19.5 km however, we set $w = 0$. We assume the shear of the vertical wind between the balloon and the gondola to be no larger than $1\,\text{m}\,\text{s}^{-1}/d_{\text{p-wake}}$. Therefore, the uncertainty in the vertical wind measurement relevant for our wake evaluation is $\Delta_w = 1\,\text{m}\,\text{s}^{-1}$. After Vaisala (2018), there is a measurement uncertainty of $\Delta_\text{RS} = 0.15\,\text{m}\,\text{s}^{-1}$ in the horizontal wind speed. Generally, self-induced motions of the balloon would add to the uncertainty in the wind measurement as well. However, the period of these self-induced balloon motions is found to be typically sufficiently below 40 s. Due to the low pass filtering of the wind data (3rd order Butterworth, 1/40 Hz cut-off frequency), the effect of these motions on the wind measurement is negligible and does not need to be considered in the error estimate. Therefore, we assume for the uncertainty in the horizontal wind:

$$\boldsymbol{\Delta_U} = \begin{pmatrix} \frac{\Delta_\text{RS}}{\sqrt{2}} \\ \frac{\Delta_\text{RS}}{\sqrt{2}} \\ \Delta_w \end{pmatrix} \tag{8}$$

In case of a LITOS launch, the uncertainty in the position of the payload $\boldsymbol{\Delta_{X_\text{p}}}$ is acquired from the motion sensor on board, from which a horizontal payload displacement $\Delta_{\text{p}_\text{horz}}$ is taken. As there is no information on the direction of the displacement available, we assume it to be equally distributed. The error on the vertical payload position is given by the vertical grid step of the radiosonde after interpolation as described in Section 3.1.1. The vertical payload displacement can be neglected because it is attached to the balloon by a string.

$$\boldsymbol{\Delta_{X_\text{p}}} = \begin{pmatrix} \frac{\Delta_{\text{p}_\text{horz}}}{\sqrt{2}} \\ \frac{\Delta_{\text{p}_\text{horz}}}{\sqrt{2}} \\ w_\text{asc}\tau \end{pmatrix} \tag{9}$$

As discussed above, the balloon is subject to self-induced horizontal motions due to aerodynamic forces in the critical and super critical Reynolds number range. They affect the balloon position at the time of wake creation. MacCready (1965) estimates the maximum amplitude of these horizontal motions to be $\Delta_{X_{\text{bal}_\text{horz}}} = 2.8 D_\text{bal}(1 + 2m_\text{r})^{-1}$, with D_bal denoting the balloon diameter and m_r the relative mass of the sphere to the displaced air. Typically, D_bal is below 10 m. In the case of the LITOS launch from 29 January 2016 (discussed in Section 3.1.4) the mean amplitude in the critical and supercrititcal Reynolds number

range is 6.3 m. The error in the vertical balloon position is given by the vertical grid step of the radiosonde after interpolation:

$$\boldsymbol{\Delta}_{\boldsymbol{X}_{\mathbf{bal}}} = w_{\mathrm{asc}}\tau \begin{pmatrix} 0 \\ 0 \\ 1 \end{pmatrix} + \frac{1}{\sqrt{2}} \begin{pmatrix} 1 \\ 1 \\ 0 \end{pmatrix} \cdot \begin{cases} 2.8 D_{\mathrm{bal}}(1+2m_{\mathrm{r}})^{-1} & \text{if } Re \geq 2 \cdot 10^5 \\ 0 & \text{if } Re < 2 \cdot 10^5. \end{cases} \tag{10}$$

In order to estimate the uncertainty in the payload-wake distance $d_{\text{p-wake}}$, we use a first order Taylor series expansion. Assuming independent variables, we obtain for the uncertainty of the payload-wake distance $\Delta_{d_{\text{p-wake}}}$:

$$\Delta_{d_{\text{p-wake}}} = \sqrt{(m\tau\boldsymbol{\Delta}_{\boldsymbol{U}})^2 + \boldsymbol{\Delta}^{\mathbf{2}}_{\boldsymbol{X}_{\mathbf{p}}} + \boldsymbol{\Delta}^{\mathbf{2}}_{\boldsymbol{X}_{\mathbf{bal}}}} \tag{11}$$

m denotes the number of timesteps between the creation of the wake and its closest encounter with the payload (c.f. Section 3.1.1).

3.1.3 Probability of wake encounter

Due to the uncertainty in the payload-wake distance $\Delta_{d_{\text{p-wake}}}$, we take a probabilistic approach to asses whether our instrument was affected by the balloon's wake. We assume the probability distribution of payload-wake distances to be Gaussian shaped. In order to assess the probability for wake encounter, we first calculate for every radial distance r between the payload and the wake centre the probability Φ that the true payload-wake distance $d_{\text{p-wake}}$ is smaller than r. Φ is given by a cumulative Gaussian distribution with a standard deviation of $\frac{\Delta_{d_{\text{p-wake}}}}{2}$ and a mean of $d_{\text{p-wake}}$ (blue curve in the right panel of Figure 3):

$$\Phi(r \,|\, d_{\text{p-wake}}, \Delta_{d_{\text{p-wake}}}) = \frac{\sqrt{2}}{\Delta_{d_{\text{p-wake}}}\sqrt{\pi}} \int_{-\infty}^{r} e^{-\frac{(y-d_{\text{p-wake}})^2}{\Delta_{d_{\text{p-wake}}}}} dy \tag{12}$$

According to Barat et al. (1984), all measurements where $d_{\text{p-wake}}$ is smaller than two balloon diameters are likely to be influenced by the balloon's wake, regardless of the balloon-gondola distance. Numerical experiments using Detached Eddy Simulation from Constantinescu and Squires (2004) however show that the width of the turbulent wake of a sphere at the relevant Reynolds numbers ($Re = 50{,}000...850{,}000$) depends on the distance to the sphere. Riddhagni et al. (1971) showed from wind tunnel measurements that the radial distribution of the probability for being in the wake is given by a cumulative Gaussian distribution (c.f. Figure 2). Therefore, we calculate the probability Ψ of being in the wake for any radial distance r to the wake centre by (red curve in the right panel of Figure 3):

$$\Psi(r \,|\, R_{\text{wake}}) = 1 - \frac{3}{R_{\text{wake}}\sqrt{2\pi}} \int_{-\infty}^{r} e^{-\frac{3(y-R_{\text{wake}})^2}{2\,R_{\text{wake}}}} dy \tag{13}$$

R_{wake} denotes the radius of the wake. According to Riddhagni et al. (1971) R_{wake} is the mean of the distribution Ψ and $R_{\text{wake}}/3$ its standard deviation. Namely, the radial distance to the wake centre with a probability for being in the wake of 50 % (FWHM). It is shown by a dashed red line in Figure 2. In z-direction, R_{wake} is approximately constant up to six diameters downstream of the sphere and grows for larger distances. This growth of the wake radius is written as (c.f. Riddhagni et al.,

1971):

$$R_{\text{wake}} = A \cdot \begin{cases} \left(\frac{d_{\text{p-bal}}}{D_{\text{bal}}}\right)^{\frac{1}{3}} & \text{if } d_{\text{p-bal}} \geq 6\, D_{\text{bal}} \\ 1 & \text{if } d_{\text{p-bal}} < 6\, D_{\text{bal}}. \end{cases} \tag{14}$$

$d_{\text{p-bal}}$ is the distance between the balloon and the payload and D_{bal} the balloon diameter. For the constant A, Riddhagni et al. (1971) gave $A = 0.7$, whereas Dommermuth et al. (2002) found $A = 0.5$ from Large Eddy Simulations. We choose $A = 0.7$ for our calculations to avoid underestimating the wake diameter.

We consider both distributions Φ and Ψ as independent of each other, because Equation 12 describes the uncertainty of the calculated payload-wake distance, whereas Equation 13 describes the intermittency of the wake. Therefore, the joint probability for a wake encounter as a function of the distance to the wake centre d is given by the product of both distributions (green line in the bottom right panel of Figure 3):

$$P_{\text{wake}}(d\,|\,R_{\text{wake}}, d_{\text{p-wake}}, \Delta_{d_{\text{p-wake}}}) = \Phi(d\,|\,d_{\text{p-wake}}, \Delta_{d_{\text{p-wake}}}) \cdot \Psi(d\,|\,R_{\text{wake}}) \tag{15}$$

The most likely distance d between the payload and the wake centre is given by the maximum in Eq. 15 (maximum of the green line in the right panel of Figure 3). Therefore, the probability for wake encounter at a given altitude is written as:

$$P_{\text{wake}}(R_{\text{wake}}, d_{\text{p-wake}}, \Delta_{d_{\text{p-wake}}}) = \max\left(\Phi(d\,|\,d_{\text{p-wake}}, \Delta_{d_{\text{p-wake}}}) \cdot \Psi(d\,|\,R_{\text{wake}})\right) \tag{16}$$

Generally, we consider every datapoint as wake-free, where the probability for wake encounter is below $P_{\text{wake}} = 5\,\%$. An example for a wake influenced data section can be seen in Figure 3. The raw velocity fluctuation data (spline subtracted) show a relatively narrow turbulent patch of 15 m with no transition from turbulent to non-turbulent regions. The wake probability in this region is comparatively high (47 %). In the spectrum of the data, we notice no clear transition from the -5/3 to the -7 range. This may be due to the inhomogeneity in the turbulence field, because the balloon does not continuously stay in the centre of the wake. The retrieved energy dissipation rate is $0.3\,\text{mW}\,\text{kg}^{-1}$. This is about one and a half orders of magnitude lower than the true atmospheric turbulence shown in Figure 1. ~~Also for the other patches of balloon-wake induced turbulence~~ We like to stress however that the data underlying Figure 1 show only one exemplary case of a turbulent altitude bin. Under different atmospheric conditions, LITOS measured atmospheric turbulence patches ranging from 0.001 $\text{mW}\,\text{kg}^{-1}$ to 100 $\text{mW}\,\text{kg}^{-1}$. In contrast, we typically find dissipation between 0.01 $\text{mW}\,\text{kg}^{-1}$ and 1 $\text{mW}\,\text{kg}^{-1}$ for balloon-wake induced turbulence. However, during previous measurements with lower payload-balloon distances we measured wake induced turbulence stronger than $10\,\text{mW}\,\text{kg}^{-1}$ (data not shown here).

3.1.4 Exemplary wake-encounter probabilities for 29 Jan 2016

The payload-wake distance $d_{\text{p-wake}}$ for the LITOS launch on 29 January 2016 is shown as a solid green line in the right panel of Figure 4. Evaluating the whole LITOS flight, we find for none of the altitude bins a wake probability of more than 95 % (considered as wake affected~~within uncertainty~~). On the other hand, 69.1 % of all altitude bins are considered wake free

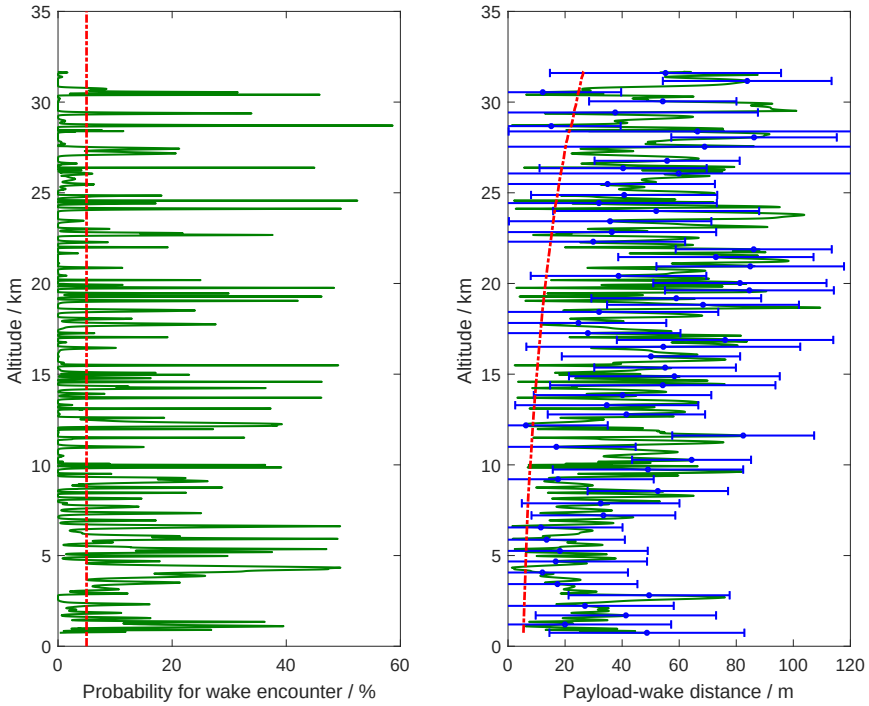

Figure 4. Wake assessment for LITOS flight on 29 Jan 2016 ($d_{\text{p-bal}} = 180$ m). Left: Probability for wake encounter on the LITOS payload (green). Probabilities smaller than 5 % are considered to be wake-free (red line). Right: Distance between the centre of the wake and the gondola ($\mathrm{d_{p\text{-}wake}}$, green line) with errorbars (blue). Upper limit for wake-free data according to Barat et al. (1984) in red. For clarity, only every 100^{th} errorbar (blue) is shown.

($P_{\text{wake}} < 5\,\%$), whereas the mean probability for a wake encounter over the whole flight is 5.6 %. According to the criterion by Barat et al. (1984), 3.5 % of all altitude bins are affected by the balloon's wake. The percentage of truly turbulent altitude bins (turbulence detected without any wake influence) for this flight however, is 6.0 %. Therefore, the occurrence rate of wake is in the same order of magnitude as the occurrence rate of atmospheric turbulence. This underlines the importance of wake identification analysis, as the wake adds a considerable amount of false turbulence detections.

3.2 Statistical evaluation of wake encounter probability

3.2.1 Influence of the payload-balloon distance for realistic soundings

We use a series of Vaisala RS41 radiosondes to evaluate typical percentages of wake influence as a function of the payload-balloon distance $d_{\text{p-bal}}$ for arbitrary payloads. This will allow users of specialised payloads to asses their risk of wake encounter.

The data set has been acquired at Kiruna in Northern Sweden during the GW-LCycle II campaign in January/February 2016. In order to consistently retrieve vertical winds, we take only those sondes into account where the uplift during the filling process was measured and a 500 g balloon has been used (30 in total). First, the vertical wind during each flight is calculated using the approach presented in Appendix A. Second, the likelihood for wake encounter is computed for every altitude bin of every radiosonde according to Section 3.1. This calculation has been done for payload-balloon distances $d_{\text{p-bal}}$ between 20 m and 200 m with a spacing of 10 m. This is possible, because instead of measuring it directly, our wake prediction algorithm calculates the wind shear between the balloon and the payload and can therefore simulate any payload-balloon distance. In contrast to the LITOS-payload, on radiosondes the angle by which the payload is displaced from the vertical is not measured. From several LITOS-flights with different payload-balloon distances we know however that the typical standard deviation of the displacement angle is around 1°, regardless of the payload-balloon distance. As the weight to cross-sectional area ratio of the LITOS-payload and the RS41 radiosonde is similar (9.8 $\mathrm{kg\,m^{-2}}$and 8.7 $\mathrm{kg\,m^{-2}}$, respectively), we assume their pendulum amplitude to be comparable, even though their shape is different. Accordingly, we use the standard deviation of the displacement angle from the LITOS measurement presented in Section 3.1.4 (0.93°). It is used for the uncertainty propagation as described in Section 3.1.2.

In Figure 5 the probabilities for wake encounter are shown. These probabilities are averaged over all altitude bins and all flights. We notice that for a balloon-gondola distance of 30 m (older radiosondes), nearly 100 % of the altitude bins are potentially wake affected ($P_{\text{wake}} > 5\,\%$) and the mean probability for wake encounter at the position of the gondola is 40 %. For a 55 m distance (currently used by Vaisala), we find approximately 4 % of all altitude bins to be certainly free of wake influence and a mean probability for wake encounter of about 28 %. For larger distances, the percentage of potentially wake influenced altitude bins decreases, reaching about 44 % for a distance of 200 m with an average wake probability of 8.8 %.

3.2.2 Influence of the payload-balloon distance and other parameters for idealised soundings

In this section, we demonstrate the quantitative influence of wind shear (Figure 6), rotation of the horizontal wind vector (Figure 7) and relative vertical balloon velocity w_{rel} (Figure 8) on the payload-wake distance $d_{\text{p-wake}}$ for different payload-balloon distances $d_{\text{p-bal}}$. For that we apply the software described in Section 3.1 on an artificial dataset with constant shear, rotation and w_{rel}, where each of these three parameters is individually and systematically changed. This dataset is based on a typical radiosonde with a 500 g rubber balloon, in line with the real data used in Section 3.2.1. In order to separate the influence of the three parameters on the wake encounter probability from instrumental effects, we did these calculations assuming an idealized instrument with no self-induced balloon motions, no pendulum motions and no measurement uncertainties of the radiosonde. Furthermore, histograms showing the frequency distribution of the above parameters are obtained from the mentioned radiosonde dataset and used to demonstrate typical values. For these histograms the respective parameter (e.g. wind shear) is calculated as a mean over the standard balloon-radiosonde distance of 55 m.

In Figure 6 we see that the risk of being in the wake increases with decreasing wind shear $d\boldsymbol{U}/dz$ and decreasing balloon-gondola distance, as expected. In this case we have assumed no rotation of the wind vector and a relative vertical balloon

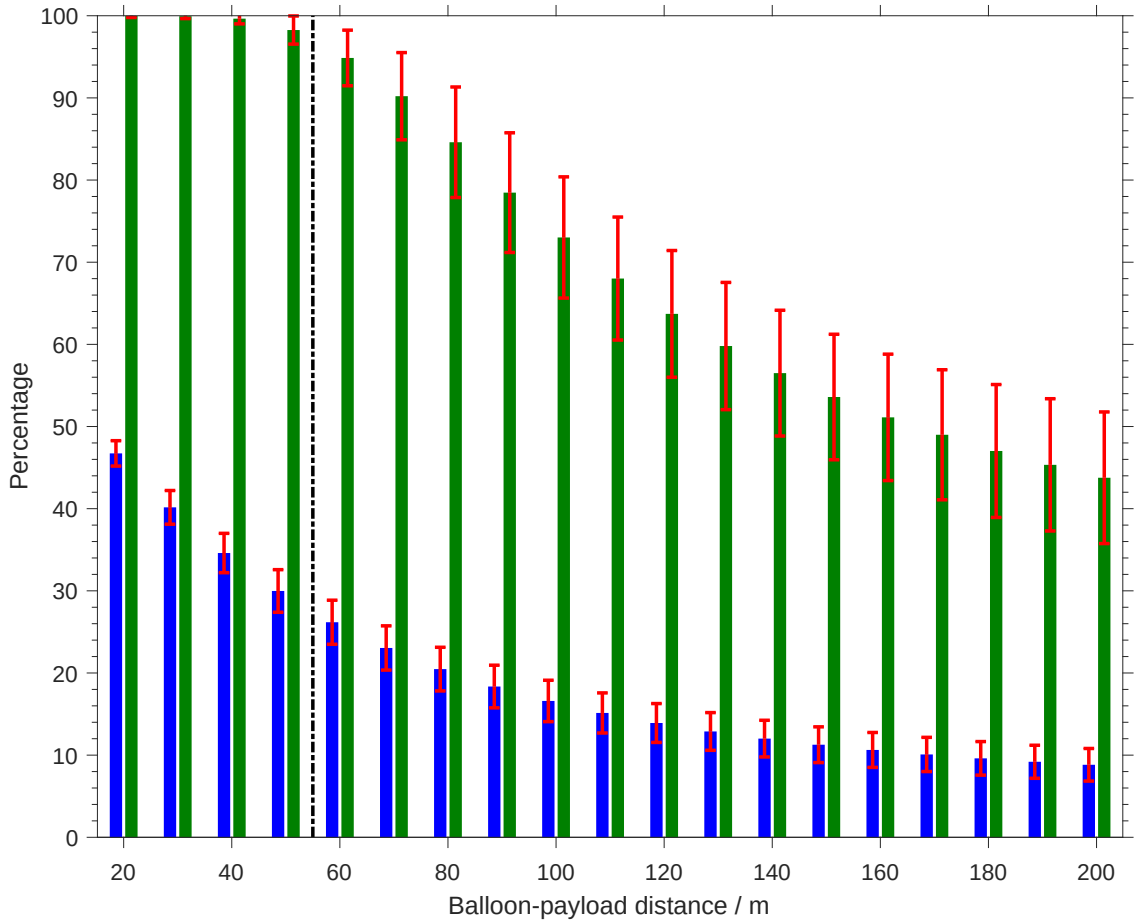

Figure 5. Blue: Mean probability of wake encounter using background information from 30 radiosondes flights. Green: Percentage of potentially wake affected altitude bins ($P_{\mathrm{wake}} > 5\,\%$). Red: Standard deviation between different launches. Black: payload-balloon distance of a standard radiosonde.

velocity of $w_{\mathrm{rel}} = 5\,\mathrm{m\,s^{-1}}$. The hatched area denotes cases with a probability for wake encounter of more than 5 %. From the plot we see that for a standard radiosonde configuration ($d_{\mathrm{p\text{-}bal}} = 55\,\mathrm{m}$) we need a wind shear of more than $12\,\mathrm{m\,s^{-1}\,km^{-1}}$ to achieve a wake probability of less than 5 %. The statistical distribution of the measurements in the right panel shows the occurrence rate of a certain shear over the payload-balloon distance of a standard radiosonde (55 m). As can be seen, these higher wind shears occur for about 30 % of all altitude bins.

Similarly, according to Figure 7 the risk of a wake encounter is reduced, if there is a rotation in the horizontal wind vector. The

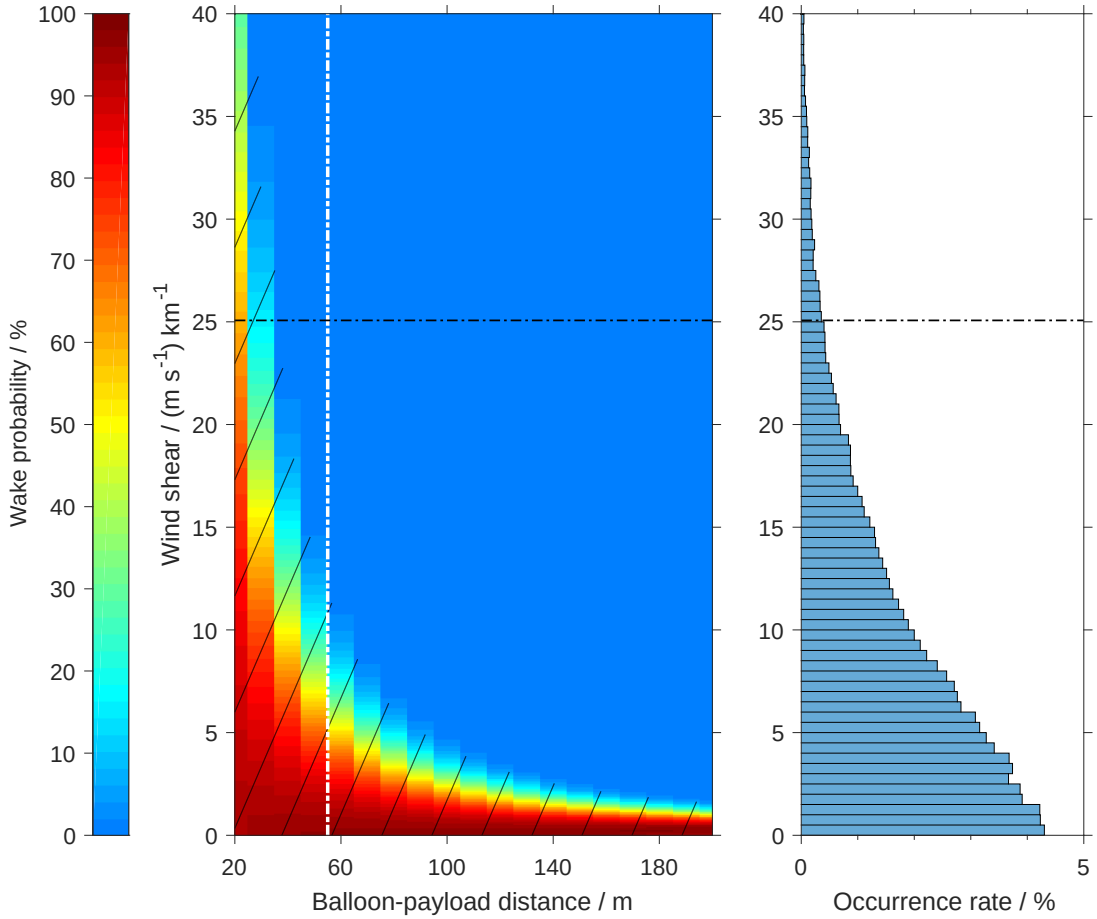

Figure 6. Wind shear influence on the wake probability P_{wake} (no wind rotation, relative vertical balloon velocity w_{rel}: $5\,\mathrm{m\,s^{-1}}$). The ninety-fifth percentile of the measured wind shear is indicated by the black dashed-dotted line. Left: Wake probability as a function of the magnitude of the wind shear and payload-balloon distance $d_{\mathrm{p\text{-}bal}}$. The white line denotes the horizontal balloon gondola distance for the RS41 radiosonde, the hatched area is potentially affected by the balloon's wake ($P_{\mathrm{wake}} > 5\,\%$). Right: Wind shear from the 30 radiosonde observations described in Section 3.2.1.

effect of a wind rotation on the payload-wake distance however, depends on the wind speed. This is, because a rotation of the wind vector leads to a larger separation of the wake and the payload for stronger wind speeds. Therefore, we plotted the wake probability as a function of the payload-balloon distance and the rotation of the horizontal wind vector multiplied by the wind speed. The dataset is created without wind shear, with a relative vertical balloon velocity of $w_{\mathrm{rel}} = 5\,\mathrm{m\,s^{-1}}$ and a typical wind

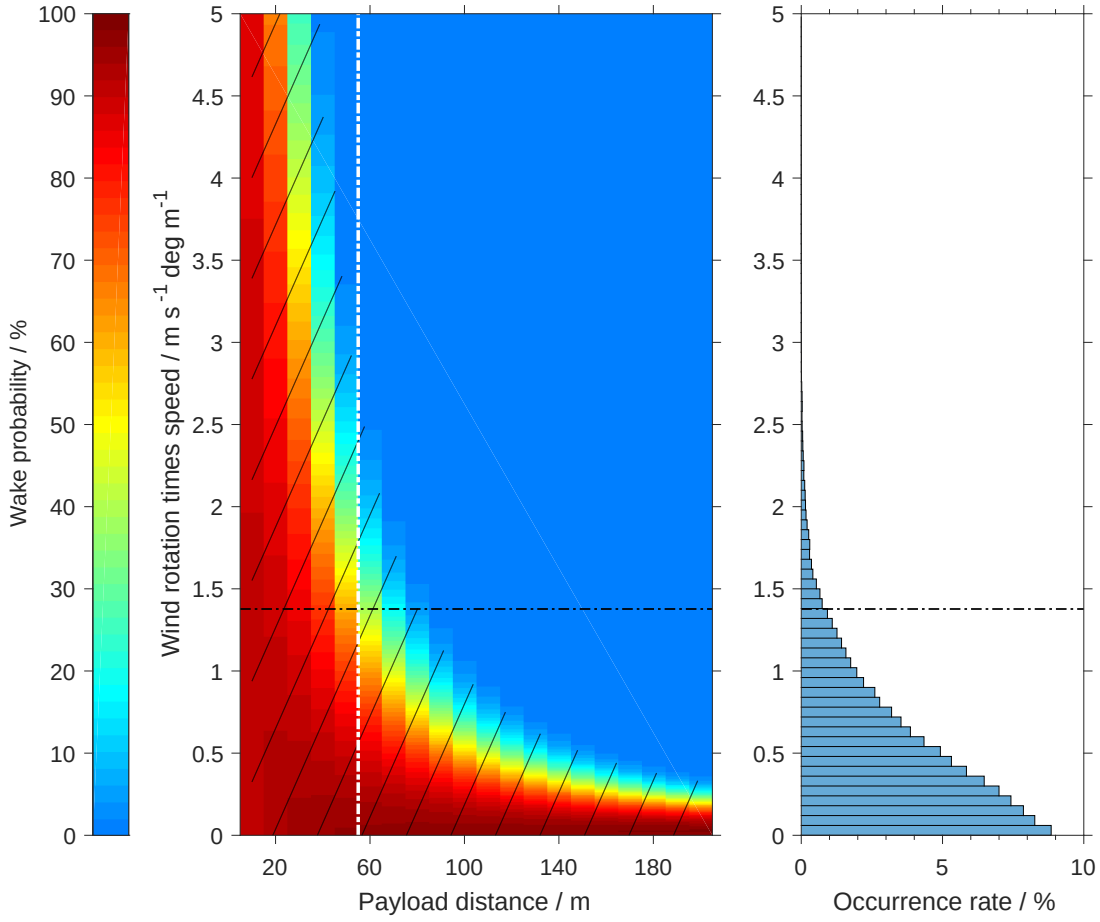

Figure 7. Same as Figure 6, but showing the influence of wind rotation on the wake probability (no wind shear, relative vertical balloon velocity w_{rel}: $5\,\mathrm{m\,s^{-1}}$).

speed of $|\boldsymbol{U}| = 20\,\mathrm{m\,s^{-1}}$. For the occurrence rate in the right panel it should be noted that the resolution of the wind direction measurement by the radiosonde is only 1°. Combined with the averaging over the $55\,\mathrm{m}$ balloon-radiosonde distance, this leads to the exceptionally high occurrence rate in the lowest bin of the right panel.

Another parameter influencing the probability for wake encounter is the relative vertical velocity between the balloon and the atmosphere w_{rel}. As expected, we find a higher probability for wake encounter for higher relative velocities (c.f. Figure 8). For our radiosonde dataset the peak of the velocity distribution is at $w_{\mathrm{rel}} = 3.5\,\mathrm{m\,s^{-1}}$.

From the analysis of these three parameters, we find that within the ~~spread of the~~ ninety-fifth percentile of the wind shear for the

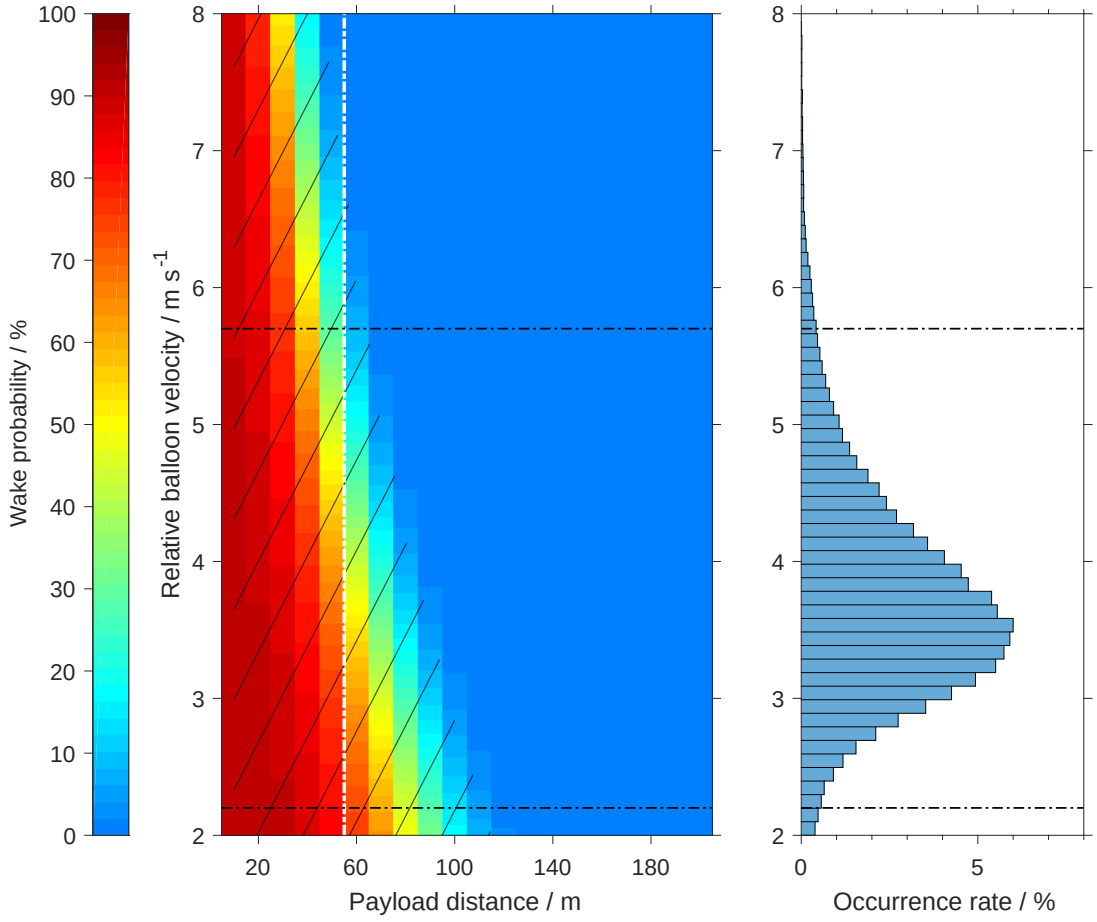

Figure 8. Same as Figure 6, but showing the influence of the relative vertical balloon velocity w_{rel} on the payload-wake distance (wind shear: $10\,\mathrm{m\,s^{-1}\,km^{-1}}$, no wind rotation).

given radiosonde dataset, the wake probability changes from 0.1 % to 96 %. Within the ninety-fifth percentile of all examined rotations in the horizontal wind vector the wake probability changes from 68 % to 95 %. For the variation in relative vertical balloon velocity the wake probability changes from 43 % to 84 %. Therefore, we conclude that within the spread of the given radiosonde dataset wind shear has the strongest influence on the likelihood for wake encounter.

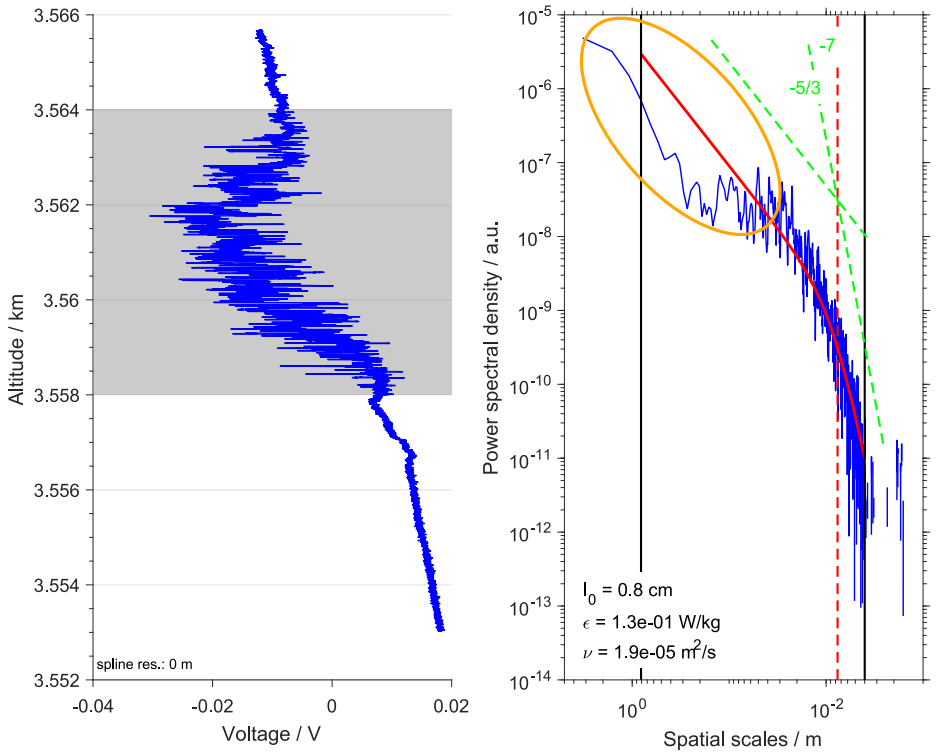

Figure 9. Wake of a rope holding the gondola. Left: Raw data from the CTA. Right: Turbulence retrieval fit as in Figure 1 from the data shown in the left panel. The orange ellipse denotes a region of reduced power spectral densities compared to the Heisenberg model (Eq. 1). This points to turbulence in the wake of a small object in the vicinity of the sensor.

4 Wake caused by the payload chain

Another possible cause for self-induced turbulence are smaller objects of sub-metre size in the payload chain above the sensor. In the case of the LITOS instrument, these are mainly the ropes holding the gondola. Both turbulence sensors used on this instrument are placed above the gondola. In the following, this will be used to exemplarily describe the effect of such an object on a high-resolution turbulence measurement.

Under unfavourable conditions, the wind shear is such that the wake of the ropes is advected to the sensors which are located below the ropes at a minimum downstream distance of 15 cm. At a rope diameter of 1 mm, the Reynolds number of the flow is between $Re = 400$ on ground level and $Re = 5$ at 32 km. For $Re > 50$ (occurring in altitudes below ~19.5 km), a Kármán vortex street forms in the flow downstream of a cylinder (Williamson, 1996; Henderson, 1995). We do not see the vortex shedding frequency in our data, which is expected because Kármán vortex streets completely break down into turbulence in the far field of the flow more than 50 diameters away from the source (Roshko, 1954; Taneda, 1959). We expect this breakdown of the

vortex street to be enhanced by the surface roughness of the rope. Consistently, strong turbulent velocity fluctuations that show a different spectral shape compared to atmospheric turbulence are seen on the CTA data if one of the sensors is hit by such a collapsed vortex street (c.f. Figure 9). For $Re < 50$, we notice a deceleration of the flow if the sensor gets into the trail of one of the ropes but no fine-scale turbulent fluctuations. This results in a different spectral shape than the one presented in Figure 9. The difference between rope-wake related and atmospheric turbulence manifests in a drop of power spectral densities at scales above $10\,\mathrm{cm}$ compared to the fit function (Eq. 1). It is explained by the measurement geometry: assuming isotropy of the turbulent flow the largest eddies can not be larger than the distance from the wake source to the sensor ($15\,\mathrm{cm}$ here), because otherwise the growth speed of the eddies would be larger than the speed of the flow around the object. Another property of these rope-wake induced turbulence is its strong local confinement: The turbulent region shown in Figure 9 has a length of only six metres along the flight track and shows a comparatively high energy dissipation rate of $130\,\mathrm{mW\,kg^{-1}}$ with hardly any transition between turbulent and non-turbulent regions.

In order to discard artificial turbulence of this kind in our LITOS retrieval we inspect every spectrum of turbulent velocity fluctuations together with its raw data by eye and discard all altitude bins that show the above mentioned distortions of the measured spectrum compared to the fit function. An automated detection does not seem feasible to us, as the changes in the spectral shape can be very subtle (presumably depending on the relative speed of the gondola w_{rel}) and are therefore difficult to capture by a criterion like the mean squared distance between the data and the fit function.

5 Discussion

Our method of measuring turbulent energy dissipation rates relies on resolving the inner scale of turbulence. Other measuring techniques determine the ~~structure function of~~ energy dissipation rate from the structure function or from the power spectral density $W(k) = A\varepsilon^{2/3}k^{-5/3}$ of the horizontal wind in the inertial subrange ~~of velocity fluctuations (Barat, 1982a)~~(Barat, 1982a, A denotes The advantage of the latter methods is that the power spectrum does not need to resolve the inner scale l_0 but can be measured at larger spatial scales. Therefore, the magnitude of the fluctuations is higher, which makes them easier to measure (c.f. Figure 1). Consequently, our method is more susceptible to wake related influences or other technical distortions due to the lower fluctuation amplitudes. On the other hand, their method requires a calibration of the anemometer that forced them to use comparatively complicated ionic anemometers (e.g. Barat, 1982b). Furthermore, our technique is more suitable on sounding balloons, because the balloon diameter (between $2\,\mathrm{m}$ and $13\,\mathrm{m}$, depending on altitude) is considerably larger than the fluctuation scales we are evaluating (order of a few centimetres). Therefore, our method avoids a filtering of measured fluctuations due to balloon movements, as reported by Barat et al. (1984). Additionally, their method depends on the assessment of parameters like the Richardson number in the turbulent layer that cannot be measured directly (Barat and Bertin, 1984a).

Considering vertical winds for the LITOS retrieval and for the payload-wake distance calculation is beneficial, because the LITOS balloon from 29 Jan 2016 as well as the radiosonde series reached ascent rate variations in the mid stratosphere of $\pm 5\,\mathrm{m\,s^{-1}}$. Assuming the balloon to show a constant relative vertical velocity w_{rel} (i.e. subtracting a mean ascent rate to obtain

the vertical wind) would result in errors of up to $\pm 2.5\,\mathrm{m\,s^{-1}}$ in w_{rel} (data not shown), compared to $\pm 1\,\mathrm{m\,s^{-1}}$ from our retrieval. Unfortunately, to our knowledge, there is no model that describes the strong variations in the vertical velocity of a balloon relative to the background vertical velocity for Reynold numbers in the critical and supercritical range. Correspondingly, a measurement of w_{rel} in the troposphere and lower stratosphere on the LITOS system using either a sonic anemometer or a Pitot tube is highly desirable.

Concerned with the significance of wake related issues for our LITOS measurements we found that turbulence induced by the balloon as well as by the ropes has substantial effects on the raw data. When comparing turbulence measurements from rising balloons to a first measurement on a descending balloon (exemplary velocity spectrum shown in Figure 1), we found several turbulent areas of only a few ten meters in altitude on the ascent data. They are suspicious for balloon-wake influence. Hence we developed the model for the propagation of the balloon-wake based on radiosonde wind data described in this paper. With respect to the verification of our wake detection algorithm we found that there is no altitude bin during the LITOS flight from 29 Jan 2016 where our model predicts a certain wake encounter (wake probability higher than 95 $\%$). This is due to the relatively large balloon gondola distance. It does not mean that no wake encounter took place. Instead, the low abundance of regions with high wake probability reflects the level of uncertainty in the calculation. Furthermore, the measured dissipation rates of balloon induced turbulence are lower than the ones created by the wake of small objects in the payload chain ($10^{-4}\,\mathrm{W\,kg^{-1}}$ vs. $10^{-1}\,\mathrm{W\,kg^{-1}}$) due to the exponential decay of turbulent intensity with time (Gibson and Lin, 1968). This means that whenever both wakes occur at the same time, the balloon's wake cannot be detected, because it is masked by the stronger wake of the ropes holding the gondola. This is the case for about one third of the dataset. When trying to identify balloon-wake related turbulence by its spectral shape, we found that it shows a less distinct transition from the inertial to the viscous subrange of the spectrum compared to atmospheric turbulence (c.f. Figure 3). This however resembles atmospheric turbulence in case of a low signal to noise ratio (occurring for low dissipation rates of $< 10^{-4}\,\mathrm{W\,kg^{-1}}$ and for low pressures of $< 100\,\mathrm{hPa}$) and therefore prevents a clear separation of balloon induced turbulence from atmospheric turbulence by its spectral shape.

Accordingly, we do not have the possibility to independently evaluate the abundance of balloon-wake related turbulence in the wake detection algorithm by comparing with the LITOS data. Nevertheless, we found many instances of agreement between the wake prediction algorithm and LITOS measurements of balloon-wake created turbulence. One of them is shown in Figure 3. For an evaluation, more launches with an improved signal to noise ratio using a LITOS version that is not affected by wake from the payload chain would be desirable.

However, we took detailed care to include all possible effects into the uncertainty assessment. This makes us confident that the calculated probability for wake encounter gives a sound estimate of the real situation. This does not hold under turbulent conditions though, because wind shears on vertical scales below $200\,\mathrm{m}$ (e.g. Barat and Bertin, 1984b) will occur. In a radiosonde measurement, these scales cannot be unambiguously resolved due to mixture with instrumental effects (pendulum motions of the gondola, bobbing motions of the balloon). Furthermore, the eddies created by the balloon will be advected by the larger eddies of the atmospheric turbulence, preventing a calculation of their path. Therefore, it is not possible to assess the payload-wake distance $d_{\mathrm{p\text{-}wake}}$ under turbulent conditions.

According to Barat et al. (1984), $d_{\text{p-wake}}$ scales with the square of the balloon-gondola distance. This strongly increases the likelihood of wake encounter for smaller payload-balloon distances. They have stated that 90 % of the data for a 2 m balloon at 100 m distance will be wake-free. From our analysis, we find that for this balloon-gondola distance of 100 m, only 27 % of all data points can be considered certainly wake-free. This value is considerably lower than the one acquired by Barat et al., even though we used a slightly smaller balloon. In contrast to their analysis we considered the measurement uncertainty in our calculation of the payload-wake distance and replaced their heuristic criterion for the minimal payload-wake distance by a consideration of the transversal shape of the wake (Riddhagni et al., 1971; Gibson and Lin, 1968). Especially important is the consideration of the self-induced balloon motions as introduced by Scoggins (1965). They substantially increase the level of uncertainty in the payload-wake distance but have not been considered by Barat et al. (1984). This is crucial, because for the largest part of a standard radiosonde ascent, the balloon will be in the critical and supercritical Reynolds number range, where these motions occur. Accordingly, we assume that our lower number of certainly wake free altitude bins is explained by the uncertainty in the wake prediction. This uncertainty is largely governed by effects inherent to sounding balloons (self-induced motions of the balloon, pendulum motions of the payload) that cannot be improved by advanced sensors.

From an analysis examining the influence of different parameters on the probability for wake encounter (Section 3.2.2) we find a strong dependence on wind shear and weaker dependencies on shears in the wind direction and on the relative velocity of the balloon. We like to stress that even though the former two cannot be influenced by the operator of the balloon, one can reduce the probability for wake encounter by reducing the ascent speed of the balloon. This will furthermore reduce the amplitude of the self-induced balloon motions.

For the LITOS system as flown on 29 Jan 2016 (balloon-gondola distance of 180 m, balloon diameter up to 13 m), we expect 69 % of the flight to be wake free. The average probability for wake encounter is 5.6 %. Earlier measurements of our group (Theuerkauf, 2012; Haack et al., 2014; Schneider et al., 2015) were conducted with a smaller balloon-gondola distance (50 m) and a larger balloon (up to 28 m) showing average wake encounter probabilities of about 60 %. Therefore, their geophysical results become questionable because of these wake related issues. Others (Schneider et al., 2017) already incorporated a precursor version of the payload-wake distance calculation that only lacked the uncertainty propagation presented here. Measurements with a critically low payload-wake distance have not been used in the latter publication, which is therefore considered to be sound within the limitations mentioned here. In order to completely avoid any wake influence we follow a technique proposed by Kräuchi et al. (2016) on all newer LITOS measurements. It features two balloons with one of them being cut away at the highest point of the flight and the other one leading to a smooth downleg with a nearly constant descent rate.

Among different balloon-borne measurements, we expect wake related turbulence to have the strongest effects on high-resolution soundings of turbulent velocity fluctuations. This is, because the wake diameter will be between one and two balloon-diameters (Constantinescu and Squires, 2004; Riddhagni et al., 1971). Therefore, the strongest turbulent motions created by a sounding balloon will be on scales below 2 m (ground level) and 26 m (top altitude, the precise value will depend on the balloon type). On the other hand, larger scale distortions occur due to the radiosonde swinging in and out of the balloon's wake (Kräuchi et al., 2016), creating another temperature signal with a period of ~ 5.5 s during nighttime and an additional signal with a period of ~ 11 s during daytime for a radiosonde-balloon distance of 30 m (Tiefenau and Gebbeken, 1989). These scales

are well resolved by the sampling rate of 1 Hz used on standard radiosondes. Therefore, Thorpe analysis results from these measurements are likely to be affected by the balloon's wake. Further experimental studies on this topic seem desirable to us. An influential wake effect on high-resolution Thorpe analysis studies can be expected (e.g. Gavrilov et al., 2005; Luce et al., 2001, spatial resolution: 10 cm, balloon-gondola distance: 100 m). Results underlining this statement come from Wilson et al. (2011). They investigate the Thorpe-analysis of standard and high-resolution radiosondes, by identifying which inversions in the measured temperature profile are caused by true atmospheric overturnings. They find that in the troposphere this is the case for only 11.4 % (25 % for high-resolution data) of all inversions. They expect the remaining inversions to be strongly influenced by instrumental noise. From our work however, we expect small scale fluctuations due to the balloon's wake to have significantly contributed to their noise estimate. This expectation is supported by Jumper and Murphy (2001) finding a considerably higher amount of small amplitude spikes in the tropospheric temperature data of the ascent compared to the wake free descent.

In addition to these temperature related effects, Kräuchi et al. (2016) report humidity measurements from standard radiosondes to be affected as well, because the balloon's skin collects moisture in the troposphere, which is subsequently released in the stratosphere leading to a patchy contamination of the measurements while the radiosonde moves in and out of the balloon's wake. Gaffen (1994) points out that for long term temperature datasets caution is required, because an increase of the balloon-radiosonde distance on newer models decreases the effect of the daytime heating of the balloon's wake, thereby leading to false cooling trends on daytime data. Luers and Eskridge (1998) note that solar radiation is a stronger concern for very short payload-balloon distances especially in the stratosphere, as the convective cooling of the temperature sensor is decreased because of the reduced relative velocity w_{res} in the wake.

Azouit and Vernin (2005) expect the wake not to have any significant effect on their measurements of the refractive index structure function constant C_N^2, which is related to atmospheric turbulence. Applying the Barat et al. (1984) criterion they find less than 2 % of all altitude bins to be affected. However, they report a mean wind shear three times as high as the one from the radiosonde dataset used here, which can explain their lower number of altitude bins with an expected balloon-wake influence.

Concerning wake influences from smaller objects in the vicinity of the sensor we notice that they can usually be identified by their spectral shape. However, if not removed from the measurement they cause false detections of strong turbulence in the order of $100\,\mathrm{mW\,kg^{-1}}$. This may be taken as a reminder that even small objects of millimetre size cause severe turbulent fluctuations up to metre-scales for at least 150 object diameters downstream of the flow disturbance.

Answering our question from the introduction: Yes, we can determine regions in the dataset that are prone to balloon-wake related measurement distortions by an automated calculation of the likelihood for balloon-wake encounter, even though there is a considerable uncertainty in the computation. Regions influenced by the wake from smaller objects in the payload chain can be identified only manually by their spectral shape of the high-resolution data.

6 Conclusions

In this article we have classified two major distortions of turbulence measurements that occur on rising balloons: Turbulence caused by the balloon and turbulence caused by small objects in the payload chain. For the former, we developed a tool to compute the likelihood of wake encounter at the payload position. This is done by calculating the drift of the balloon's wake using radiosonde data and applying a full uncertainty analysis. However, such an assessment is generally not possible under turbulent conditions due to the advection of the balloon's wake. The uncertainty has been reduced by adapting the vertical wind retrieval from Wang et al. (2009) to our larger balloons and to the different launch preparation procedures. Furthermore, we developed a statistical approach to approximate the size of the wake that is based on laboratory studies. We found instances of good agreement between our balloon-wake prediction and the LITOS data. The abundance of these wake encounters however cannot be unambiguously evaluated, because the balloon's wake is masked for about one third of the flight due to turbulence created by small objects. The latter was found to be not accessible to an automatic detection. Instead, we sort those areas out by manual inspection of the spectral shape of all turbulent altitude bins.

By analysing a set of 30 radiosondes with our wake assessment tool we found that for a standard radiosonde configuration only about 4 % of the flight can be certainly considered wake free, with an average wake probability of about 28 %. The low abundance of certainly wake free regions also reflects the uncertainty in the wake assessment, which is largely caused by motions inherent to sounding balloons. From a general perspective, measurements resolving scales in the centimetre range or below will be additionally susceptible to the wake of small objects like our ropes. Our study shows however that the wake of large objects like the balloon will influence measurements of standard radiosondes with meter scale resolution as well. Deduction of atmospheric turbulence parameters from radiosonde balloons can be seriously flawed if wake effects are ignored. This calls for thorough investigations of wake effects on sounding balloon measurements and for even longer payload-balloon distances than the 55 m currently used on standard radiosondes. For research purposes where the complete avoidance of any wake influence is crucial (e.g. turbulence measurements, high accuracy temperature soundings), we strongly recommend to measure on a descending balloon with the sensor pointing downward.

7 Data and source code availability

The MATLAB® source code for the wake evaluation tool (Section 3.1) and for the vertical wind retrieval (Appendix A1) is published online at ftp://ftp.iap-kborn.de/data-in-publications/Soeder2018AMT/.

Besides the source code, this repository contains a user guide and the data underlying Figure 4 as a running example. The radiosonde data used in Section 3.2.1 can be obtained via the HALO database (https://halo-db.pa.op.dlr.de/mission/3). The LITOS data and more specialised source code will be made available on request to the corresponding author.

Appendix A: Vertical wind retrieval from radiosonde data

A1 Calculation of vertical winds

For the retrieval of energy dissipation rates from the LITOS instrument and for our wake prediction algorithm we need to obtain the relative vertical velocity w_{rel} between the balloon and the sonde. Since LITOS does not measure vertical winds, we retrieve them from the ascent rate of the radiosonde instead. The variations of ascent rate however, are not directly proportional to the vertical wind, because of changing flow conditions around the balloon (e.g. Gallice et al., 2011). We follow the approach of Wang et al. (2009), who obtained vertical winds by using a parametrisation of the balloon ascent based on the balance of the drag force and the buoyancy force of the balloon. We measure the lift of our balloon during the filling with an uncertainty of $\pm 5\,\mathrm{N}$. In the data post processing, we optimise the value for the balloon lift at launch and the drag coefficient of the balloon such that the median of the retrieved vertical wind is minimal (criterion based on Wang et al., 2009). For easier comparison, our article adopts the notation of Wang et al. (2009).

In more detail, we write the buoyancy force of the balloon BF as the difference of the lifting force and the accumulated weight force due to the masses of the payload (m_{p}), the balloon (m_{b}) and the lifting gas (helium, m_{He}):

$$\mathrm{BF} = g\mathrm{BV}\rho - g(m_{\mathrm{p}} + m_{\mathrm{b}} + m_{\mathrm{He}}), \tag{A1}$$

where g denotes the gravitational constant, ρ the air density and BV the balloon volume, which can be expressed using the balloon volume at launch BV_0 and the air density at launch ρ_0 by $\mathrm{BV} = \mathrm{BV}_0\rho_0/\rho$. Furthermore, the helium mass can be expressed in terms of the helium density on ground level (ρ_{He}) by $m_{\mathrm{He}} = \mathrm{BV}_0\rho_{\mathrm{He}}$. Therewith, the balloon volume at launch is written as:

$$\mathrm{BV}_0 = \frac{\mathrm{BF}_0/g + m_{\mathrm{b}}}{\rho_0 - \rho_{\mathrm{He}}}, \tag{A2}$$

BF_0 is the lifting force of the balloon at launch. We measure the lifting force of our balloon during the filling process BF_{f} inside a hangar with an uncertainty of $\pm 5\,\mathrm{N}$. Inside the hangar, we find a different temperature T_{f} compared to the outside temperature at launch T_0. This leads to a non-adiabatic loss in balloon volume and lifting force during the subsequent launch preparations outside the hangar. Assuming ideal gas law ($\mathrm{BV}_0 = \mathrm{BV}_{\mathrm{f}}\frac{T_0}{T_{\mathrm{f}}}$), we rewrite Equation A1 for the buoyancy force of the balloon using Equation A2:

$$\mathrm{BF} = (gm_b + \mathrm{BF}_{\mathrm{f}})\frac{T_0}{T_{\mathrm{f}}} - g(m_{\mathrm{p}} + m_{\mathrm{b}}), \tag{A3}$$

As mentioned above, during flight the buoyancy force BF equals the drag force DF of the balloon. The latter is given by:

$$\mathrm{DF} = (c_{\mathrm{db}}A_{\mathrm{b}} + c_{\mathrm{dp}}A_{\mathrm{p}})\rho w_{\mathrm{rel}}^2/2. \tag{A4}$$

c_{db} denotes the drag coefficient of the balloon, A_{b} its cross-sectional area and w_{rel} the relative vertical velocity between the balloon and the surrounding air. c_{dp} stands for the drag coefficient of the payload and $A_{\mathrm{p}} = 0.5\,\mathrm{m}^2$ for the accumulated cross-sectional area of all payload boxes in the case of LITOS. The shapes of the payload boxes include cuboids, spheres and cones.

We assume their drag coefficient to be $c_{\mathrm{dp}} = 1$ on average. Accordingly, balancing the buoyancy force and the drag force of the balloon and using Equation 2 yields for the vertical wind:

$$w = w_{\mathrm{asc}} - \sqrt{2\mathrm{BF}/((c_{\mathrm{db}}A_{\mathrm{b}} + c_{\mathrm{dp}}A_{\mathrm{p}})\rho)} \tag{A5}$$

From this equation, in combination with Equation A3, c_{db} and BF_{f} are fitted so that the median of all retrieved vertical winds w over the whole flight is minimised (approach similar to Wang et al., 2009). The drag coefficient c_{db} however, depends on the flow conditions around the balloon. These flow conditions are characterised by the Reynolds number:

$$Re = \frac{w_{\mathrm{rel}} D_{\mathrm{bal}}}{\nu}, \tag{A6}$$

w_{rel} is the relative vertical velocity between the balloon and the atmosphere, D_{bal} is the balloon diameter and ν the kinematic viscosity according to Equation 4. As w_{rel} is a result of the vertical wind retrieval, we need to make an initial guess for Re by assuming that $w = 0$ and therefore $w_{\mathrm{rel}} = w_{\mathrm{asc}}$. In a second run, Re is calculated as described in Equation A6 and shown in the left panel of Figure A1 using a cut-off period of 40 s to remove bobbing motions of the balloon (caused by the flexibility of the balloon material), self-induced motions of the balloon and pendulum motions of the payload. For the initial guess, all changes in ascent rate due to changing aerodynamic forces on the balloon are removed by a digital low pass filter with a cut-off period of 400 s.

The resulting ascent rate in still air is shown by the black line in the right panel of Figure A1. The resulting subcritical drag coefficient is $c_{db} = 0.56$, which is slightly higher than the 0.50 to 0.51 obtained by Achenbach (1974) for smooth and marginally roughened spheres. The resulting lifting force is 75 N. The remaining median of the vertical wind (fit residuum) is $2 \cdot 10^{-10}\,\mathrm{m\,s^{-1}}$. Wang et al. (2009) found a mean fit residuum of $0.02\,\mathrm{m\,s^{-1}}$ for 102 radiosondes launched during the Terrain-induced Rotor Experiment (T-Rex) in 2006. This shows a sufficient fit quality in our adapted version of the model. For comparison of our retrieved vertical winds we use the Weather Research and Forecasting (WRF) model with a horizontal resolution of 800 m (setup similar to Schneider et al. (2017)). We compare the vertical from our retrieval algorithm with vertical winds winds from the model along the flightpath of the radiosonde. In the critical and supercritical Reynolds number range (below $\approx 19\,\mathrm{km}$ altitude) this model shows vertical winds of up to $\pm 2\,\mathrm{m\,s^{-1}}$ along the flight track (not shown here), while our retrieval assumes $w = 0$. Therefore, the error of setting $w = 0$ is below $\pm 2\,\mathrm{m\,s^{-1}}$ in our case. In the subcritical Reynolds number range (above $\approx 19\,\mathrm{km}$ altitude) the deviation between retrieved vertical winds and model data is below $1\,\mathrm{m\,s^{-1}}$ for altitudes below 26 km. Above, the amplitudes of the model decrease sharply, possibly caused by the damping layer of the model starting at 30 km altitude. As a rough guess, we may estimate the error in the vertical wind above 19.5 km to be below $\pm 1\,\mathrm{m\,s^{-1}}$.

We are aware that there are effects influencing the ascent rate that are not included in the model. Presumably, the most important one is a temperature difference of the lifting gas to the surrounding air. Gallice et al. (2011) developed an extensive model considering the temperature distribution of the lifting gas inside the balloon. However, according to the authors it is applicable to night time launches only and needs an experimentally acquired drag curve for the particular balloon type. Both conditions make their calculations unsuitable to our dataset.

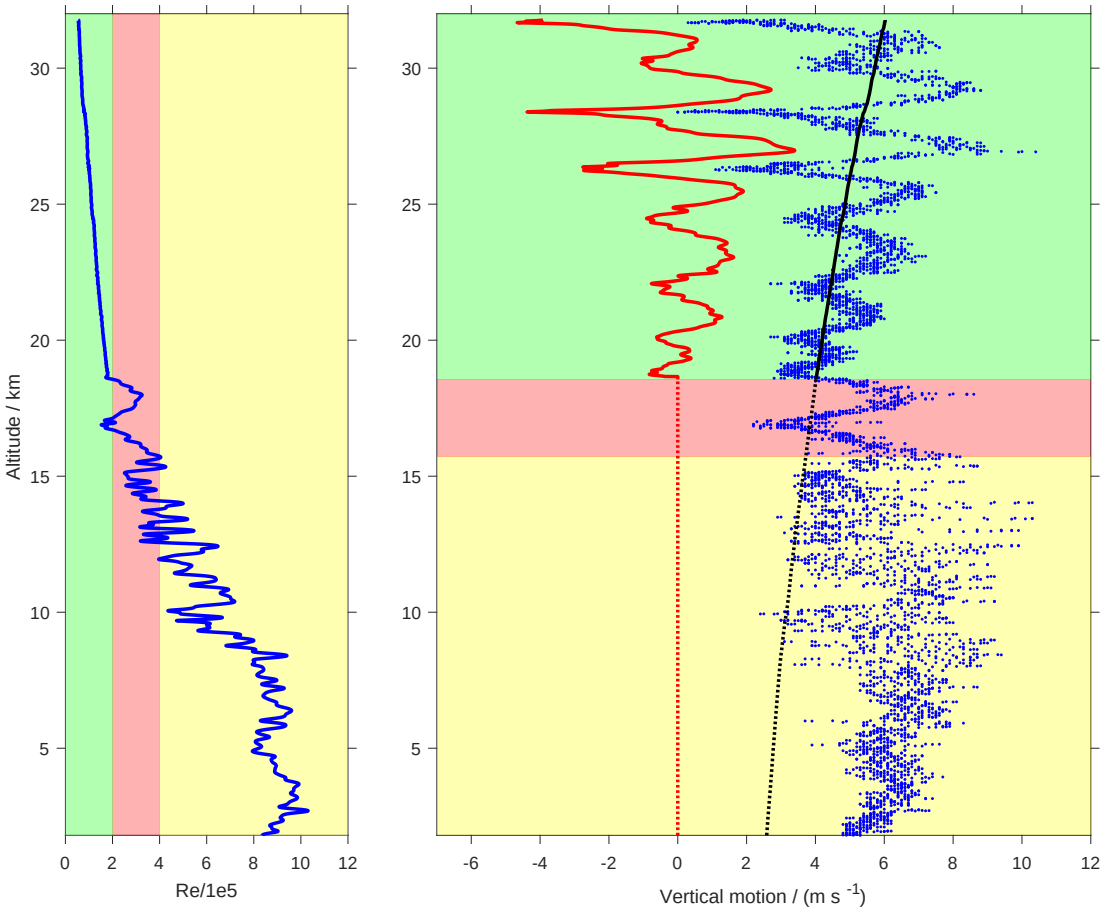

Figure A1. Left: Reynolds number of the flow around the balloon according to Equation A6. Right: unfiltered ascent rates of the balloon (blue dots). Relative vertical velocity of the balloon w_{rel} (black), vertical winds according to Equation A5 (red). Vertical winds in the supercritical and critical Reynolds number regime are set to zero because of changing drag coefficients. Retrieved relative vertical velocities underestimate the ascent rates in these regimes and are shown as a dashed black line. Both panels: Subcritical (green), critical (red) and supercritical (yellow) flow regime.

Author contributions. JS acquired LITOS evaluated the LITOS data, prepared the software and wrote the manuscript with feedback from the other authors. MG supervised the acquisition of the LITOS data and contributed to the discussion of the manuscript. AS provided parts of the software that is used to retrieve energy dissipation rates. AD supported the discussion of the manuscript and supervised the GW-LCycle measurement campaign under which the radiosonde data series and part of the LITOS data used here have been acquired. HW contributed to the discussion of the manuscript and the uncertainty estimate in the wake evaluation tool in particular. JW set up the WRF simulations that

are used as a comparison for the vertical wind retrieval. FJL took part in the discussion of the manuscript and provided the general concept behind the LITOS measurement.

Competing interests. The authors declare that they have no conflict of interest.

Acknowledgements. We like to thank Christoph Zülicke and Mark Schlutow for countless insightful discussion on the subject of this publication. Moreover, we acknowledge the help of Reik Osterman and Michael Priester with the development of the LITOS instrument.

We greatly appreciate the funding received from the Bundesministerium ~~für~~ für Bildung und Forschung (BMBF, Federal Ministry of Education and Research) under project 01 LG 1218A (ROMIC-METROSI). The radiosonde data used in this study have been acquired during the GW-LCycle II campaign of the project 01 LG 1206A (ROMIC-GWLcycle). Many fruitful discussions on the subject were made possible in the framework of the MS-GWaves project by the Deutsche Forschungsgemeinschaft (DFG, German Research Foundation). Last but not least we like to thank Richard Wilson and one anonymous referee for their comments and Jörg Gumbel for handling the manuscript.

References

Achenbach, E.: The effects of surface roughness and tunnel blockage on the flow past spheres, Journal of Fluid Mechanics, 65, 113–125, doi:10.1017/S0022112074001285, 1974.

Aßmann, R.: Über die Existenz eines wärmeren Luftstromes in der Höhe von 10 bis 15 km, Sitzungsbericht der Königlich-Preußischen Akademie der Wissenschaften zu Berlin, 24, 495–504, 1902.

Azouit, M. and Vernin, J.: Optical Turbulence Profiling with Balloons Relevant to Astronomy and Atmospheric Physics, Publications of the Astronomical Society of the Pacific, 117, 536, http://stacks.iop.org/1538-3873/117/i=831/a=536, 2005.

Barat, J.: Some Characteristics of Clear-Air Turbulence in the Middle Stratosphere, Journal of the Atmospheric Sciences, 39, 2553–2564, doi:10.1175/1520-0469(1982)039<2553:SCOCAT>2.0.CO;2, 1982a.

Barat, J.: Initial Results from the Use of Ionic Anemometers Under Stratospheric Balloons: Application to the High-Resolution Analysis of Stratospheric Motions, Journal of Applied Meteorology, 21, 1489–1496, doi:10.1175/1520-0450(1982)021<1489:IRFTUO>2.0.CO;2, 1982b.

Barat, J. and Bertin, F.: Simultaneous Measurements of Temperature and Velocity Fluctuations Within Clear Air Turbulence Layers. Analysis of the Estimate of Dissipation Rate by Remote Sensing Techniques, Journal of the Atmospheric Sciences, 41, 1613–1619, doi:10.1175/1520-0469(1984)041<1613:SMOTAV>2.0.CO;2, 1984a.

Barat, J. and Bertin, F.: On the Contamination of Stratospheric Turbulence Measurements by Wind Shear, Journal of the Atmospheric Sciences, 41, 819–828, doi:10.1175/1520-0469(1984)041<0819:OTCOST>2.0.CO;2, 1984b.

Barat, J., Cot, C., and Sidi, C.: On the Measurement of the Turbulence Dissipation Rate from Rising Balloons, Journal of Atmospheric and Oceanic Technology, 1, 270–275, doi:10.1175/1520-0426(1984)001<0270:OTMOTT>2.0.CO;2, 1984.

Bouttier, F. and Kelly, G.: Observing-system experiments in the ECMWF 4D-Var data assimilation system, Quarterly Journal of the Royal Meteorological Society, 127, 1469–1488, doi:10.1002/qj.49712757419, 2001.

Clayson, C. A. and Kantha, L.: On Turbulence and Mixing in the Free Atmosphere Inferred from High-Resolution Soundings, Journal of Atmospheric and Oceanic Technology, 25, 833–852, doi:10.1175/2007JTECHA992.1, 2008.

Constantinescu, G. and Squires, K.: Numerical investigations of flow over a sphere in the subcritical and supercritical regimes, Physics of Fluids, 16, 1449–1466, doi:10.1063/1.1688325, 2004.

Dommermuth, D. G., Rottman, J. W., Innis, G. E., and Novikov, E. A.: Numerical simulation of the wake of a towed sphere in a weakly stratified fluid, Journal of Fluid Mechanics, 473, 83–101, doi:10.1017/S0022112002002276, 2002.

Gaffen, D. J.: Temporal inhomogeneities in radiosonde temperature records, Journal of Geophysical Research: Atmospheres, 99, 3667–3676, doi:10.1029/93JD03179, 1994.

Gallice, A., Wienhold, F. G., Hoyle, C. R., Immler, F., and Peter, T.: Modeling the ascent of sounding balloons: derivation of the vertical air motion, Atmospheric Measurement Techniques, 4, 2235–2253, doi:10.5194/amt-4-2235-2011, 2011.

Gavrilov, N. M., Luce, H., Crochet, M., Dalaudier, F., and Fukao, S.: Turbulence parameter estimations from high-resolution balloon temperature measurements of the MUTSI-2000 campaign, Annales Geophysicae, 23, 2401–2413, https://hal.archives-ouvertes.fr/hal-00329429, 2005.

Gibson, CH Chen, C. and Lin, S.: Measurements of turbulent velocity and temperature fluctuations in the wake of a sphere., AIAA Journal, 6, 642–649, doi:10.2514/3.4557, 1968.

Gong, J. and Geller, M. A.: Vertical fluctuation energy in United States high vertical resolution radiosonde data as an indicator of convective gravity wave sources, Journal of Geophysical Research: Atmospheres, 115, doi:10.1029/2009JD012265, 2010.

Haack, A., Gerding, M., and Lübken, F.-J.: Characteristics of stratospheric turbulent layers measured by LITOS and their relation to the Richardson number, Journal of Geophysical Research: Atmospheres, 119, 10,605–10,618, doi:10.1002/2013JD021008, 2014.

Heisenberg, W.: Zur statistischen Theorie der Turbulenz, Zeitschrift für Physik, 124, 628–657, 1948.

Henderson, R. D.: Details of the drag curve near the onset of vortex shedding, Physics of Fluids, 7, 2102–2104, doi:10.1063/1.868459, 1995.

Jang, Y. I. and Lee, S. J.: PIV analysis of near-wake behind a sphere at a subcritical Reynolds number, Experiments in Fluids, 44, 905–914, doi:10.1007/s00348-007-0448-2, https://doi.org/10.1007/s00348-007-0448-2, 2008.

Jumper, G. and Murphy, E.: Effect of balloon wake on thermosonde results, in: 32nd AIAA Plasmadynamics and Lasers Conference, p. 2796, doi:10.2514/6.2001-2796, 2001.

Kräuchi, A., Philipona, R., Romanens, G., Hurst, D. F., Hall, E. G., and Jordan, A. F.: Controlled weather balloon ascents and descents for atmospheric research and climate monitoring, Atmospheric Measurement Techniques, 9, 929–938, doi:10.5194/amt-9-929-2016, 2016.

Kyrazis, D. T., Eaton, F. D., Black, D. G., Black, W. T., and Black, A.: The balloon ring: a high-performance low-cost instrumentation platform for measuring atmospheric turbulence profiles, in: Atmospheric Optics: Models, Measurements, and Target-in-the-Loop Propagation III, vol. 7463, p. 746308, International Society for Optics and Photonics, doi:10.1117/12.827540, 2009.

Lalas, D. P. and Einaudi, F.: Tropospheric gravity waves: Their detection by and influence on rawinsonde balloon data, Quarterly Journal of the Royal Meteorological Society, 106, 855–864, doi:10.1002/qj.49710645014, 1980.

Luce, H., Fukao, S., Yamamoto, M., Sidi, C., and Dalaudier, F.: Validation of Winds Measured by MU Radar with GPS Radiosondes during the MUTSI Campaign, Journal of Atmospheric and Oceanic Technology, 18, 817–829, doi:10.1175/1520-0426(2001)018<0817:VOWMBM>2.0.CO;2, 2001.

Luce, H., Fukao, S., Dalaudier, F., and Crochet, M.: Strong Mixing Events Observed near the Tropopause with the MU Radar and High-Resolution Balloon Techniques, Journal of the Atmospheric Sciences, 59, 2885–2896, doi:10.1175/1520-0469(2002)059<2885:SMEONT>2.0.CO;2, 2002.

Luers, J. K. and Eskridge, R. E.: Use of Radiosonde Temperature Data in Climate Studies, Journal of Climate, 11, 1002–1019, doi:10.1175/1520-0442(1998)011<1002:UORTDI>2.0.CO;2, 1998.

Lübken, F.-J.: On the extraction of turbulent parameters from atmospheric density fluctuations, Journal of Geophysical Research: Atmospheres, 97, 20 385–20 395, doi:10.1029/92JD01916, 1992.

MacCready, P. B.: Comparison of Some Balloon Techniques, Journal of Applied Meteorology, 4, 504–508, doi:10.1175/1520-0450(1965)004<0504:COSBT>2.0.CO;2, 1965.

Murrow, H. N. and Henry, R. M.: Self-Induced Balloon Motions, Journal of Applied Meteorology, 4, 131–138, doi:10.1175/1520-0450(1965)004<0131:SIBM>2.0.CO;2, 1965.

NOAA: US standard atmosphere, 1976, Tech. rep., NOAA-S/T, 1976.

Reeder, M. J., Adams, N., and Lane, T. P.: Radiosonde observations of partially trapped lee waves over Tasmania, Australia, Journal of Geophysical Research: Atmospheres, 104, 16 719–16 727, doi:10.1029/1999JD900038, 1999.

Riddhagni, P., Bevilaqua, P., and Lykoudis, P.: Measurements in the turbulent wake of a sphere, AIAA Journal, 9, 1433–1434, doi:10.2514/3.6379, 1971.

Roshko, A.: On the development of turbulent wakes from vortex streets, Tech. Rep. 1191, California Institute of Technology, https://ntrs.nasa.gov/archive/nasa/casi.ntrs.nasa.gov/19930092207.pdf, 1954.

Schneider, A.: In-situ turbulence observations in the stratospheric wind and temperature field, dissertation, Universität Rostock, https://www.iap-kborn.de/fileadmin/user_upload/MAIN-abteilung/optik/Forschung/Doktorarbeiten/Schneider-Diss-2015.pdf, 2015.

Schneider, A., Gerding, M., and Lübken, F.-J.: Comparing turbulent parameters obtained from LITOS and radiosonde measurements, Atmospheric Chemistry and Physics, 15, 2159–2166, doi:10.5194/acp-15-2159-2015, 2015.

Schneider, A., Wagner, J., Söder, J., Gerding, M., and Lübken, F.-J.: Case study of wave breaking with high-resolution turbulence measurements with LITOS and WRF simulations, Atmospheric Chemistry and Physics, 17, 7941–7954, doi:10.5194/acp-17-7941-2017, 2017.

Scoggins, J. R.: Spherical Balloon Wind Sensor Behavior, Journal of Applied Meteorology, 4, 139–145, doi:10.1175/1520-0450(1965)004<0139:SBWSB>2.0.CO;2, 1965.

Scoggins, J. R.: Sphere behavior and the measurement of wind profiles, Tech. rep., NASA, Washington, D.C., https://ntrs.nasa.gov/archive/nasa/casi.ntrs.nasa.gov/19670017960.pdf, 1967.

Sharman, R., Cornman, L., Meymaris, G., Pearson, J., and Farrar, T.: Description and derived climatologies of automated in situ eddy-dissipation-rate reports of atmospheric turbulence, Journal of Applied Meteorology and Climatology, 53, 1416–1432, 2014.

Sharman, R. D. and Pearson, J. M.: Prediction of Energy Dissipation Rates for Aviation Turbulence. Part I: Forecasting Nonconvective Turbulence, Journal of Applied Meteorology and Climatology, 56, 317–337, doi:10.1175/JAMC-D-16-0205.1, 2017.

Shutts, G. J., Kitchen, M., and Hoare, P. H.: A large amplitude gravity wave in the lower stratosphere detected by radiosonde, Quarterly Journal of the Royal Meteorological Society, 114, 579–594, doi:10.1002/qj.49711448103, 1988.

Survo, P., Turunen, M., Salo, T., and Jauhiainen, H.: VAISALA RADIOSONDE RS41–NEW SENSING TECHNOLOGIES FOR OPERATIONAL UPPER AIR MEASUREMENTS, https://www.wmo.int/pages/prog/www/IMOP/publications/IOM-116_TECO-2014/Session%201/O1_4_Survo_VaisalaRS41.pdf, 2014.

Taneda, S.: Downstream Development of the Wakes behind Cylinders, Journal of the Physical Society of Japan, 14, 843–848, doi:10.1143/JPSJ.14.843, 1959.

Taneda, S.: Visual observations of the flow past a sphere at Reynolds numbers between 10^4 and 10^6, Journal of Fluid Mechanics, 85, 187–192, doi:10.1017/S0022112078000580, 1978.

Theuerkauf, A.: Stratospheric turbulence observation with the new balloon-borne instrument LITOS, dissertation, Universität Rostock, https://www.iap-kborn.de/fileadmin/user_upload/MAIN-abteilung/optik/Forschung/Doktorarbeiten/Theuerkauf-Diss-2012.pdf, 2012.

Theuerkauf, A., Gerding, M., and Lübken, F.-J.: LITOS – a new balloon-borne instrument for fine-scale turbulence soundings in the stratosphere, Atmospheric Measurement Techniques, 4, 55–66, doi:10.5194/amt-4-55-2011, 2011.

Tiefenau, H. K. E. and Gebbeken, A.: Influence of Meteorological Balloons on Temperature Measurements with Radiosondes: Nighttime Cooling and Daylight Heating, Journal of Atmospheric and Oceanic Technology, 6, 36–42, doi:10.1175/1520-0426(1989)006<0036:IOMBOT>2.0.CO;2, 1989.

Vaisala: Vaisala Radiosonde RS41-SG – accuracy and reliability, Vaisala Corporation, https://www.vaisala.com/sites/default/files/documents/RS41-SG-Datasheet-B211321EN.pdf, 2018.

Wang, J., Bian, J., Brown, W. O., Cole, H., Grubišić, V., and Young, K.: Vertical Air Motion from T-REX Radiosonde and Dropsonde Data, Journal of Atmospheric and Oceanic Technology, 26, 928–942, doi:10.1175/2008JTECHA1240.1, 2009.

Williamson, C. H.: Vortex dynamics in the cylinder wake, Annual Review of Fluid Mechanics, 28, 477–539, doi:10.1146/annurev.fl.28.010196.002401, 1996.

Wilson, R., Luce, H., Dalaudier, F., and Lefrère, J.: Turbulence Patch Identification in Potential Density or Temperature Profiles, Journal of Atmospheric and Oceanic Technology, 27, 977–993, doi:10.1175/2010JTECHA1357.1, 2010.

Wilson, R., Dalaudier, F., and Luce, H.: Can one detect small-scale turbulence from standard meteorological radiosondes?, Atmospheric Measurement Techniques, 4, 795–804, doi:10.5194/amt-4-795-2011, 2011.